9-24-2018

Evaluation of the BSC-DREAM8b Regional Dust Model Using the 3D LIVAS-CALIPSO Product

Dimitra Konsta
National Observatory of Athens

Ioannis Binietoglou
National Institute of R&D for Optoelectronics, Romania

Antonis Gkikas
National Observatory of Athens

Stavros Solomos
National Observatory of Athens

Eleni Marinou
National Observatory of Athens

See next page for additional authors

Recommended Citation

Konsta, D., Binietoglou, I., Gkikas, A., Solomos, S., Marinou, E., Proestakis, E., Basart, S., García-Pando, C. P., El-Askary, H., and Amiridis, V.: Evaluation of the BSC-DREAM8b regional dust model using the 3D LIVAS-CALIPSO product, Atmos. Environ., 195, 46-62, doi:10.1016/j.atmosenv.2018.09.047, 2018.

Evaluation of the BSC-DREAM8b Regional Dust Model Using the 3D LIVAS-CALIPSO Product

Authors
Dimitra Konsta, Ioannis Binietoglou, Antonis Gkikas, Stavros Solomos, Eleni Marinou, Emmanouil Proestakis, Sara Basart, Carlos Pérez García-Pando, Hesham el-Askary, and Vassilis Amiridis

Evaluation of the BSC-DREAM8b regional dust model using the 3D LIVAS-CALIPSO product

Dimitra Konsta[1], Ioannis Binietoglou[2], Antonis Gkikas[1], Stavros Solomos[1], Eleni Marinou[1,3], Emmanouil Proestakis[1], Sara Basart[4], Carlos Pérez García-Pando[4], Hesham El-Askary[5,6,7] and Vassilis Amiridis[1]

[1] IAASARS, National Observatory of Athens, 15236 Athens, Greece

[2] National Institute of R&D for Optoelectronics, Magurele, Romania

[3] Institut für Physik der Atmosphäre, Deutsches Zentrum für Luft- und Raumfahrt (DLR), Oberpfaffenhofen, Germany

[4] Earth Sciences Department, Barcelona Supercomputing Center, Barcelona, Spain

[5] Center of Excellence in Earth Systems Modeling & Observations, Chapman University, Orange, CA, 92866, USA

[6] Schmid College of Science and Technology, Chapman University, Orange, CA, 92866, USA

[7] Department of Environmental Sciences, Faculty of Science, Alexandria University, Moharem Bek, Alexandria, 21522, Egypt

Abstract

The ability of regional atmospheric models to accurately represent long-range transport of dust is crucial for describing dust effects on radiation and clouds and for reducing their uncertainties on these processes. The optimized CALIPSO (Cloud-Aerosol Lidar and Infrared Pathfinder Satellite Observations) pure-dust product that provides the three-dimensional patterns of dust and its transport pathways is a unique tool that can address the aforementioned model's issues. In this study we use the CALIPSO dust extinction profiles as a tool for examining the performance of the regional dust model BSC-DREAM8b in space and time, for the period 2009-2013 over Northern Africa, the Mediterranean, Europe, Eastern North Atlantic and the Middle East. Our analysis suggests that the model overestimates the dust extinction coefficient above dust source regions in Sahara Desert especially at altitudes lower than 3km at about 0.04 km^{-1}. We also found a slight underestimation of transported dust over Europe and Atlantic Ocean lower than 0.025km^{-1} of extinction coefficient values all along the vertical column. Over the Mediterranean dust is overestimated (~0.01km^{-1}) in layers higher than 1 km height. Dust in the Middle East is significantly underestimated by the model (~0.05km^{-1}) all along the vertical column especially during warm seasons. The study also provides an analysis of the CALIPSO limitations and uncertainties on the detection of strong dust activity contributing to the

differences between the simulations and observations above the dust sources of Bodelé and Algeria.

1. Introduction

Mineral dust is one of the most abundant aerosol types on the Earth's atmosphere, emitted from wind erosion and soil resuspension over arid and semiarid regions. It travels in the free troposphere from one day to one week depending on its size, and then deposit by sedimentation, wet or dry deposition [Colarco et al., 2003]. Dust aerosols affect the radiative balance both directly (by interacting with shortwave and longwave radiation, Sokolik et al., 2001, Perez et al. 2006, Balkanski et al., 2007) and indirectly (by acting as cloud condensation and ice nuclei, DeMott et al., 2003). Three-dimensional dust models are important tools for studying the complete dust lifecycle including emission, transportation and deposition near or far from the sources. Hence, they have been widely used both at global [e.g., Ginoux et al., 2004; Mikami et al., 2006; Zhu et al., 2007] and regional [e.g., Perez et al., 2006; Klein et al., 2010; Solomos et al., 2011] scales.

Despite notable advances in modeling, dust remains the dominant factor in the uncertainty of aerosol radiative forcing [Myhre et al., 2013]. Soil dust characteristics, primarily from the Saharan and Middle East Deserts, have changed since the pre-industrial era due to i) land disturbance and resulting desertification and ii) changes in climate. Recent studies by Mahowald et al., 2010 and Mulitza et al., 2010, found that the dust load, emission and deposition has increased over the 20th century, concomitant with the development of agriculture. At the same time, analysis of dust sources [Ginoux et al., 2010], suggests that a significant fraction of transported dust has an anthropogenic origin [Chen et al., 2017; Zhang et al., 2017] and along with mineral dust particles emitted from natural processes affect the Earth's albedo. Considerable research efforts have been devoted to quantify dust directive radiative forcing [Park and Jeong, 2008; Huang et al., 2009; Chen et al., 2017]. However, there is no full estimate of the resulting radiative forcing due to dust particles [Myhre et al., 2013].

The vertical distribution of aerosols is one of the main sources of uncertainties regarding their impact on the Earth-atmosphere system's radiation budget [Textor et al., 2006, Samset et al., 2013; Kipling et al., 2015]. This is attributed to the misrepresentation of the atmospheric processes (e.g. dust emission rates, turbulence, convection, planetary boundary layer (PBL) height, heating and buoyancy changes of dust layers) in the models governing aerosols' three dimensional structure [Kipling et al., 2013; 2015]. Therefore, the accurate representation of dust vertical distribution is much needed to i) improve the representation of dust life cycle components (i.e. transport and deposition) and ii) to assess dust radiation interactions and the subsequent impacts on atmospheric dynamics from short (weather) to long (climate) term temporal scales. The deposition processes are of particular importance for the marine biota of the Mediterranean Sea, Red Sea and the Atlantic Ocean [Markaki et al., 2003; Li et al., 2017].

Sufficient altitude-resolved information on aerosols abundance and properties has been lacking. However, significant progress in characterizing the tropospheric aerosol vertical distribution has been made in recent years through the deployment of ground and satellite

based lidar measurements. From space, vertically resolved aerosol and cloud observations are acquired from the Cloud-Aerosol Lidar and Infrared Pathfinder Satellite Observations (CALIPSO) since mid-June 2006 [Winker et al., 2010]. Specifically, CALIPSO is established as an accurate and robust mean for mineral dust identification from space [Liu et al., 2008; Omar et al., 2009]. The 3-D LIVAS (Lidar climatology of Vertical Aerosol Structure) -CALIPSO pure-dust dataset developed by Amiridis et al. [2015] provides the horizontal and vertical patterns of Saharan dust loads over Europe [Marinou et al., 2017]. The aerosol height information provided at high vertical resolution by the CALIOP extinction profiles is vital for validating source strengths and improving aerosol radiative forcing calculations in dust models.

BSC-DREAM8b model has been already evaluated in previous dust model evaluation studies revealing the principle model's biases. Basart et al., [2012] used Aerosol Optical Depth (AOD) retrievals from AERONET to evaluate BSC-DREAM8b model stating that the model underestimates AOD over the Sahel during winter and overestimates AOD over the Middle East and the Mediterranean region for 2004. In accordance with these results, Amiridis et al. [2013], who relied on CALIPSO and AERONET measurements, reported that the BSC-DREAM8b model overestimates dust over Europe, the Mediterranean and the Atlantic Ocean, while it underestimates dust loads over source areas in North Africa. Binietoglou et al., [2013] found that the model is reproducing adequately the shape of dust profiles but underestimates the concentration levels at 10 ACTRIS/EARLINET stations located in Europe. Moreover, the EARLINET station operating in Potenza (southern Italy) was used by Mona et al., [2014] to evaluate the simulated dust extinction profiles showing that the model underestimates dust abundance, particularly at the lowest tropospheric levels (below 3km).

This study uses the 3-D pure dust CALIPSO product to evaluate the capability of BSC-DREAM8b dust model to simulate the mineral dust vertical distribution. The paper is structured as follows. In section 2 we present the main characteristics of the model and the pure dust product as well as the applied methodology performed for the evaluation of model outputs against observations. In section 3 we present and discuss the obtained findings while in section 4 summary is made and the main conclusions are drawn.

2. Methodology

2.1. The BSC-DREAM8b dust model

The Dust Regional Atmospheric Model (DREAM) has been initially developed as an additional aerosol module for the Eta model [Nickovic et al., 2001] to simulate and predict the atmospheric cycle of mineral dust aerosols. It is based on the Euler-type partial differential nonlinear equation for dust mass continuity and is operated by the National Center for Environmental Prediction's Global Forecast System (NCEP)/Eta atmospheric model [Janjic, 1977, 1979, 1984, 1990, 1994, 1996a, 1996b; Mesinger et al., 1988; Zhao

and Carr, 1977]. The concentration equation simulates all major processes of the atmospheric dust cycle. During the model integration, calculation of the surface dust injection fluxes is made over the model's cells declared as deserts. Once injected into the air, dust aerosol is driven by the atmospheric model processes, namely, a) turbulence in the early stage of the process when dust is lifted from the ground to upper levels; b) winds in the later phases of the process when dust travels away from the sources; c) thermodynamic processes and rainfall of the atmospheric model; and d) land cover features which provide wet and dry deposition of dust (including impaction, gravitational sedimentation, interception, Brownian and turbulent coagulation) over the Earth surface.

It is noteworthy that the updated version of the model, BSC-DREAM8b v2 [Pérez et al., 2006; Basart et al., 2012] is developed and operated at the Barcelona Supercomputing Center, Spain (BSC; http://www.bsc.es/projects/earthscience/BSC-DREAMess/bsc-dust-daily-forecast). Its operational forecasts is also participating in the Northern Africa–Middle East–Europe (NA-ME-E) node of the World Meteorological Organization (WMO) Sand and Dust Storm Advisory and Assessment System (SDS-WAS; https://sds-was.aemet.es/). This updated version by the model includes an approximation of the dust size distribution of eight size bins within the radius range between 0.1-10μm [Tegen and Lacis, 1996], considers dust interactive radiative feedbacks [Pérez et al., 2006]; improved dust source representation, and updated wet and dry deposition schemes. The model has been evaluated and tested against observations [e.g., Jiménez-Guerrero et al., 2008; Pay et al., 2010; Basart et al., 2012; Gama et al., 2015], in source regions during SAMUM-1 [Haustein et al., 2009] and the Bodelé Dust Experiment [BoDEx; Todd et al., 2008].

For the present study, the model configuration used for the present study includes 24 Eta vertical layers extending up to approximately 15 km in the vertical. The resolution is set to 0.33º x 0.33º in the horizontal. For each bin the extinction coefficient is calculated at 550 nm with a Mie-algorithm as described in Perez et al. [2006]. The period of study extends from 1st January 2009 to 31 December 2013 and the temporal resolution of the model outputs is 1 h. The domain of simulation covers northern Africa, the Middle East and Europe. The Final Analyses of the National Centers of Environment Prediction (NCEP/FNL; at 1º × 1º) at 00 UTC were used every 24 h as initial conditions and boundary conditions at intervals of 6 h. The model does not include dust data assimilation and the initial state of the dust variables is defined by the 24-h of the previous-day model run, except in the cold start when model dust concentration is initialized to zero. The 'cold start' of the model is initiated on 27 December of 2008.

2.2. The CALIPSO pure-dust product

CALIOP measures aerosol backscatter profiles at 532nm and 1064nm, at high horizontal and vertical resolution [Winker et al., 2009]. For the BSC-DREAM8b evaluation, we use the optimized CALIPSO pure-dust product that discriminates the pure-dust component from the total aerosol load by applying three corrections on the standard CALIPSO dust extinction retrievals [Amiridis et al., 2013]. Firstly, the pure-dust backscatter coefficient component is

decoupled from the total aerosol backscatter to separate pure dust in external aerosol mixtures, based on a depolarization technique [Tesche et al., 2009]. A correction is then applied based on an averaging scheme that includes zero extinction values for the non-dust aerosol types detected. Finally, the pure dust extinction coefficient is estimated using a spatially constant lidar ratio (i.e. extinction-to-backscatter ratio) of 55 sr instead of 40 sr used in CALIPSO v3 [Omar et al., 2009]. The selection of the 55 sr LR is based on long-term EARLINET (European Aerosol Research Lidar Network) measurements [Papayannis et al., 2008; Pappalardo et al., 2010] of Saharan dust plumes over Europe, which is applied to individual Level 2 dust-related backscatter products over cloud free profiles. Specifically for the region of Middle East (30-50^{o} E and 0-40 ^{o} N) the lidar ratio of 40 sr is preserved due to the different mineralogy of Arabian sources [Nisantzi et al., 2015]. The extinction coefficient profiles at 532nm are vertically integrated to estimate the Dust Optical Depth (DOD). The quality control procedure follows the CALIPSO L3 version 3 screening procedure [Tackett et al., 2018], and additional filters are applied to ensure the use of cloud-free profiles only [Marinou et al., 2017]. This product has been used to provide the three-dimensional distribution of dust and the dust transport pathways across northern Africa and Europe [Marinou et al., 2017], Asia [Proestakis et al., 2017], as well as in a synergistic approach with dust models for the description of severe events [Solomos et al., 2017] and impacts of dust on radiative transfer [Tsikerdekis et al., 2017].

The CALIPSO pure-dust product describes satisfactorily the dust properties, although due to the CALIPSO orbital characteristics and to laser attenuation the product is subjected to specific limitations. Such a limitation is presented in Appendix A that shows the DOD calculated from the pure dust CALIPSO product (Fig. Aa) and the total daily mean Aerosol Optical Depth (AOD) observed from MODIS (Moderate Resolution Imaging Spectroradiometer) at 1°x1° grid resolution and collocated over the CALIPSO overpasses for the period 2009-2013 (Fig. Ab). As expected, the maps show that the MODIS AOD is almost everywhere higher than CALIPSO DOD, especially in northern latitudes, since MODIS measures total AOD, so all aerosol types are taken into account, including anthropogenic and biomass burning aerosols above Europe.

When focusing over northern Africa and the Middle East, where dust is the predominant aerosol type, CALIPSO detects lower values of DOD compared to MODIS. This difference is maximized over the dust sources situated in Bodelé, Algeria and Libya. In particular, over the dust source regions of northwestern Africa MODIS detects AOD values almost twice greater than CALIPSO DOD, while over the Northern Chad region the difference is maximized where CALIPSO measures DOD of about 0.3 and MODIS detects AOD values of 1.2(Fig. A). This discrepancy has already been documented in the literature. Ma et al. [2013] have shown that CALIPSO AOD is systematically lower than MODIS AOD over major dust regions, with maximum observed departures over the Sahara. CALIPSO does not satisfactorily detect strong dust activities over the main sources of Bodelé, Algeria and Libya. Yu et al. [2010] compared CALIPSO observations with GOCART model simulations and MODIS retrievals and found that in dust source regions GOCART extinction is larger than CALIOP observations by a factor of 2 or more. Kittaka et al. [2011] compared AOD derived from CALIPSO with MODIS Aqua AOD and found that AOD from CALIPSO has a small global mean relative to MODIS. Comparison studies of CALIPSO AOD with measurements at AERONET sites showed a negative CALIPSO bias [Schuster et al., 2012; Omar et al., 2013].

For satellite measurements, it remains challenging to distinguish heavy dust loading from clouds, because of the usually large overlap of optical properties between them. Over or close to source regions heavy dust might be misclassified as clouds. Another significant source of uncertainty in the retrieved profile occurs in layers with optical depth greater than about 3, when the lidar signal is completely attenuated, which might be the case in large dust events [Kosmopoulos et al., 2017; Solomos et al., 2017]. Both cases bias the aerosol extinction to a lower magnitude [Yu et al., 2010]. Despite these known limitations of dust underestimation above the dust generation regions, the CALIPSO pure-dust product is trustworthy over the adjacent regions of dust sources and the regions of dust transport. CALIPSO product is able to observe aerosols' vertical structure over unfavorable surfaces and at night, to distinguish dust from non-dust aerosols and thus can be satisfactorily used for model evaluation taking into consideration the aforementioned cautions.

2.3. Comparison Methodology

For evaluation purposes we utilize the extinction coefficient profiles from the pure dust CALIPSO product [Amiridis et al., 2013]. Model outputs are bilinearly interpolated in space and linearly interpolated in time to CALIPSO overpasses so that the model profiles used in the analysis correspond exactly in space and time with the CALIPSO footprints. The derived profiles are then interpolated over the CALIPSO vertical coordinates. Both CALIPSO and the model collocated outputs are then regridded to a horizontal resolution of 1°x1° for the period of study (2009-2013) to be consistent for the present analysis. The observed and simulated variables used for the evaluation are the dust extinction coefficient profiles, the DOD and the dust center of mass height which is calculated as shown in Equation 1:

$$CoM = \frac{\int_{z_t}^{z_b} za(z)dz}{\int_{z_t}^{z_b} a(z)dz} \quad (1)$$

where z_b and z_t denote the base and top altitude of the dust and a denotes the dust extinction coefficient at altitude z (above sea level). To avoid cases with low dust extinction coefficient that bias the center of mass to high altitudes, which is the case here, we applied an empirical threshold by setting the dust extinction coefficient to be greater than 0.001.

The following statistical indicators are implemented in the comparison analysis between the observed and the simulated variables, as defined in Binietoglou et al., [2012]:

- The mean bias (MB), defined as:
  $MB = \frac{1}{N}\sum_{i=1}^{N}(Mi - O_i)$ (2),
  where M and O represent the simulated and the observed variables respectively for the i th measurement pair. The mean bias shows the averaged over- and underestimation of the simulated values. It ranges from -∞ to ∞ and its perfect score is 0.

- The fractional bias (F_B):
  $F_B = \frac{2}{N}\sum_{i=1}^{N}\left(\frac{M_i - O_i}{M_i + O_i}\right)$ (3),

where the bias is a normalized measure of the mean bias excluding cases where prominent outliers occur. It varies between -2 and +2 and its perfect score is 0.

- The correlation coefficient (r)

$$r = \frac{\sum_{i=1}^{N}(M_i - \acute{M})(O_i - \acute{O})}{\left[\sum_{i=1}^{N}(M_i - \acute{M})^2 \sum_{i=1}^{N}(O_i - \acute{O})^2\right]^{\frac{1}{2}}} \quad (4)$$

measures the strength and direction of the linear relationship between the simulated and the observed variables and quantifies their correlation and dependence. It ranges from -1 to 1 and its perfect score is 1.

- The root mean square error (RMSE)

$$RMSE = \left[\frac{1}{N}\sum_{i=1}^{N}(M_i - O_i)^2\right]^{\frac{1}{2}} \quad (5)$$

quantifies the sample standard deviation of the differences, representing the average distance between the simulated and the observed data. It is a measure of how spread out the simulated from the observed values are, it ranges from 0 to ∞ and its perfect score is 0.

All the above statistical indicators correspond to time and are estimated in each 1°x1° grid-cell. The obtained results presented in the geographical distribution correspond to long term temporal scales (i.e. annual, seasonal). At a regional level, the statistics are representative both at temporal and spatial scales.

3. Results and Discussion

3.1. Evaluation of columnar mean dust properties

In this section, we evaluate the column-integrated dust optical depth and the center of mass of dust layers simulated by the BSC-DREAM8b model against real observations obtained from CALIOP. Figure 1 shows the spatial distribution of Dust Optical Depth (DOD) derived by the CALIPSO dust product (Fig. 1a), simulated by BSC-DREAM8b (Fig. 1b) and the statistical indicators (MB, r, RMSE and F_B) over the study region. The long-term averaged maps as well as the corresponding evaluation metrics are representative for the period 2009-2013.

The intercomparison between CALIOP (Fig. 1a) and model DODs values (Fig. 1b) reveals that the DOD is well reproduced by the BSC-DREAM8b model both in spatial and temporal terms. More specifically, the simulated dust activity is more intense over the dust

source regions of Bodelé, Mali-Mauritania, Algeria and across the Arabian Peninsula's deserts. Likewise, moderate DOD values (~0.2) are simulated over the adjacent regions of the eastern part of the tropical Atlantic Ocean and the Mediterranean, regions that are frequently affected by the dust transport. During the study period, there is an evident covariance between simulated and observed DODs with r values higher than 0.7 over the dust sources and over areas affected by short-to-medium range dust transport (Fig. 1e). This agreement diminishes towards the northern parts of the study region (i.e. northern to 40º N), where long range dust transport takes place. The geographical distribution of MB (Fig. 1c) shows that the model underestimates (~ 0.1) dust loads at southern latitudes (southern to 20º N) and the Arabian Peninsula, while it simulates more dust with respect to CALIPSO (~0.4) over Bodelé, Algeria and Libya. This discrepancy is probably attributed to CALIOP's deficiency to detect strong dust activity over the aforementioned regions. In Northern Europe, the MB is zero associated with low DOD values. However, the F_B (Fig. 1d) takes high values, although the differences between model and observations are small, showing that there is an overestimation of dust in northwestern Europe and the adjacent Atlantic region, while the underestimation is maximized (F_B~1.5) over Northern Africa. The RMSE shows greater values (>0.4) in the regions with the strongest dust activity across the Sahara Desert and the Middle East in which the maximum distance error between observations and model, particularly over North Africa, is also found (Fig. 1f).

The representativeness of the model results is checked in Appendix B (Fig. B). The first column of Figure B presents the evaluation of DOD following Fig. 1 (i.e. using the model outputs collocated to CALIPSO overpasses). In the second column (Fig. Bb,f,j) we present the evaluation of DOD without applying any collocation criteria. When all model outputs are considered, more dust (~0.1 AOD) is simulated by the model, leading to an overestimation across African regions (including source areas) as well as in the Mediterranean. When looking at the difference between the observed and simulated values (Fig. Bi-j), for the regions of Sahara southern to 20°N the model overestimates dust (~0.2) when considering all the model outputs, while it underestimates it (~ -0.1) when considering only the collocated outputs. This shows that the model-observations intercomparison findings varies depending on when collocated or not-collocated approach is followed, due to the sampling frequency of CALIPSO (provides about two measurements per grid per month) and this should be taken into consideration in relevant studies. In addition, the day-night time differences both for the observations and for the model are examined in Appendix B (Fig. B third and fourth column respectively). Slight differences between day and night are reported (<0.1 AOD), both for the observed and simulated dust extinction. These differences do not affect the model evaluation, though CALIPSO detects slightly more dust during nighttime. On the contrary the model seems to simulate slightly more dust during daytime over the Algerian desert with higher values of DOD of around 0.6, compared to the maximum simulated values of 0.5 during night time. Moreover, the model captures the variability between day and night due to the activation of the dust sources in contrast to CALIPSO. This leads to an overestimation (underestimation) of the simulated dust load during daytime (nighttime).

The evaluation of the model's performance has been also analyzed on a seasonal basis. Figure 2 presents the spatial distribution of the dust optical depth among seasons: January to March (JFM), April to June (AMJ), July to September (JAS) and October to December (OND), following Marinou et al., [2017]. The CALIPSO dust product (Fig. 2 a-d) shows that dust activity is intense during spring with high DOD values of about 0.5 over the Northwestern Africa dust sources of Mali and Mauritania. During summer months (JAS) dust activity is strongest above

the Sahara dust sources (~0.6) in accordance with previous studies [Rodriguez et al., 2015; Knippertz and Todd, 2010]. A decrease in the dust activity (DOD <0.2) is observed during autumn (OND), while in winter period (JFM) dust activity is low but still present. The Arabian Peninsula presents also intensive dust activity all year long, but the DOD is relatively low during autumn and winter compared to other seasons and presents maximum values during spring and summer.

The model captures the seasonal patterns of dust with the simulated dust activity growing strong in spring and summer and weakening in autumn (Fig.2 e-h) over the area of study. The shift from southern latitudes during autumn and winter to northern latitudes in spring and summer is also reproduced by the model following the ITCZ position [Prospero et al., 1981] as well as the location of the most active dust sources [Prospero et al., 2002, Ginoux et al., 2012]. The general conclusions regarding the model evaluation on annual basis are still present in the seasonal evaluation (Fig. 2 i-p): the model overestimates dust optical depth across the northwestern parts of Sahara above the Atlas mountain range and underestimates it above southern Sahara, whereas both declinations reveal a seasonal variability. More precisely, the aforementioned biases are maximized in spring (AMJ) when dust loads are higher and weaken during autumn (OND). Throughout the year, the MB shows that dust transport over the Mediterranean and Europe is well simulated by the model, while F_B indicates an overestimation of transported dust over Europe (F_B~ 1), especially during autumn and winter (Fig. 2m,p). During spring and summer the overestimation is less important, while on the eastern Europe, the Balkans and Turkey the model underestimates dust (F_B~-1, Fig. 2n,o). In sub-Sahel regions (0-15º N) the model underestimates the dust optical depth especially during spring by about 0.2 (Fig. 2j). This underestimation is less pronounced in winter and summer while during autumn the optical depth is slightly overestimated (by about 0.05). Throughout the year, the model simulates weak dust transport towards the Eastern Tropical North Atlantic (0-30°N), while it simulates satisfactorily the transport of dust over the Eastern Subtropical North Atlantic (30-60°N). There is also a significant underestimation of dust emission over the Arabian Peninsula, being stronger (~0.2) during spring and weaker (~0.05) during autumn. In autumn (Fig. 2l,p) the model slightly overestimates AOD (overestimation<0.1) almost all over the area (with the exception of Northern Atlantic and the Arabian Peninsula), while the relative overestimation is important over northern Africa (F_B~1.5).

Then the dust center of mass height is evaluated. Fig. 3a presents the mean annual distribution of the dust CoM height, showing that the core of mineral particles' load within the troposphere is recorded at 1.5 km above Northern Africa reaching up to 2.5km over Bodelé, Algeria and the Arabian Peninsula due to strong convection [Engelstaedter and Washington, 2007]. The CoM height gradually decreases in northern and southern latitudes, found at 1.5 km, 1.0 km, and lower than 0.5 km over the Mediterranean, Southern and Northern Europe, respectively, and at ~1km over southern Sub-Sahel regions, attributed to diffusion and deposition processes and being in agreement with previous analyses relied on EARLINET observations [Papayannis et al., 2008]. Even though the model simulates the general pattern, the agreement with respect to the observations exhibits a spatial variation (Fig. 3B-d). More specifically, it is evident a slight overestimation of dust CoM height over the Arabian Peninsula (~0.25km), while all over the Mediterranean, Europe and the adjacent Atlantic Ocean, the model simulates lower dust CoM heights (~0.05km). Over Africa the model simulates satisfactorily the dust height with a slight underestimation (<0.2km). The correlation between the observed and simulated CoM heights (Fig. 3e) is very good (>0.85) in low latitudes (< 40°N) and decreases

over Northern Europe. The pattern of the dust center of mass correlation coefficient is similar to the DODs (Fig. 1e) as the model has difficulties in simulating the long-range dust transport. The RMSE presents uniform values of ~1km with the exception of central Africa where the error is lower (~0.2km), the Mediterranean and the adjacent Ocean (RMSE~1.5km).

The seasonal evaluation of the geographical distribution of the dust center of mass is presented in Figure 4. The center of mass according to CALIPSO (Fig. 4 a-d) reaches high heights above the dust source regions of Sahara in Northern Africa and above the Arabian Peninsula being gradually decreased over the adjacent regions of transport over the Atlantic Ocean and the Mediterranean Sea. The center of mass varies also with season, with higher and lower heights during the warm period (JAS) and during autumn (OND), respectively. Over the Sahara, particularly at its eastern parts, the center of mass reaches 3 km height during JAS. Over the Mediterranean Sea and southern Europe, the main portion of the dust layer is traveling at ~ 2 km in spring and summer and at ~1 km height during autumn and winter months.

The model (Fig. 4 e-p) also simulates the main features of the dust center of mass with the biases presented in the following. The biases persist all year but are more or less pronounced according to the season. To be more specific, the model underestimates the height of the center of mass above North Africa and the adjacent Atlantic Ocean at the order of 1 km during spring and summer and at the order of 0.5 km during autumn and winter months. It underestimates the dust CoM in northern latitudes over the Mediterranean Sea and Europe (~0.5km) during spring and summer months, and less than 0.5 km during autumn and winter. Over Morocco and the Arabian Peninsula, the model overestimation of the dust center of mass height is less than 1km, this overestimation being stronger during warm months.

3.2. Evaluation of vertical dust distribution

To evaluate the vertical distribution of dust simulated by the BSC-DREAM8b at a regional scale, the study area has been divided in four longitudinal zones extending from 22 to 60º N (Fig. 5a-d): 22 to 10º W (corresponding to Northeastern Atlantic), 10º W to 10º E (Western Sahara, Western Mediterranean and Northwestern Europe), 10 to 30º E (Eastern Sahara, Eastern Mediterranean and Northwestern Europe) and 30 to 50º E (Middle East). Figure 5 presents for each region the zonal mean profile of the dust extinction coefficient as observed by the CALIPSO dust product, as simulated by the model as well as the mean and fractional bias defined as model-observations.

The CALIPSO dust product reveals patterns of the dust cycle (emission and transport) over the area (Fig. 5e-h). It shows that dust is ubiquitous present at heights close to the surface from 0 to 40º N. Near the Saharan dust sources (10 – 25º N) increased dust activity is observed while mineral particles reach up to 6 km. When moving from west to east the top height of dust is decreasing, as it has been presented also for the broader Mediterranean region [Gkikas et al., 2016]. The model is in good agreement with the observations, simulating the general pattern of dust vertical profiles but biases are also present. It overestimates the dust near the sources and underestimates the dust layers around the sources, i.e. adjacent to the surface, southern the sources (0-15º N), above the sources (at about 4-6km) as well as northern of them (northern of

35º N), while the absolute bias is always low (<±0.2). More specifically, for the area between 22º to 10º W over the Atlantic Ocean (Fig.5a,e,i,m,q) the presence of elevated dust plumes is observed for latitudes up to 30º N reaching up to 5 km and yields high values of extinction coefficient (up to 0.09 km^{-1}) over Africa. The model underestimates this plume by simulating lower values of extinction (0.05km^{-1}) across the Africa region especially at low layers, but also in higher altitudes by missing the high elevated layers (~ 5km). This underestimation is not apparent in the fractional bias (Fig. 5q). A small overestimation (of about 0.02 km^{-1}) is found at heights of 0.5 - 2 km across the dust sources of Western Africa (Fig. 5m). Over the area of 10º W to 10º E, high values of extinction are observed (around 0.12 km^{-1}) above North Africa and the Algerian desert (Fig. 5f). In those regions dust is elevated up to 6km. Dust is transported further to higher latitudes towards the Mediterranean and central Europe. In northern regions (30 – 50º N), the values of extinction are decreased (~0.02 km^{-1}) but are still present at ~1km height. The model underestimates the extinction coefficient in southern latitudes (0 - 15 ºN) both in intensity (up to 0.06 km^{-1}) and height (up to 6 km), the greatest underestimation found in low altitudes all over the African zone (Fig. 5 j-r). On the contrary, there is an overestimation of the extinction (of about 0.03 km^{-1}) above the Algerian desert. Moving eastwards (10 – 30º E), similar patterns are observed. Dust extinction over the dust sources of central Sahara and Libya reaches values of 0.11 km^{-1} close to the surface while dust extinction over the western Mediterranean is around 0.30 km^{-1} (Fig. 5g). Dust is also trapped by the topography and washed out by precipitation at eastern Alps and the Carpathian Mountains, preventing its transport to the north. It reaches high altitudes (up to 6 km) above the sources and decreases with increasing distance from the dust sources. The model simulates higher values of dust extinction above the Saharan sources of around 0.12 km^{-1} (Fig. 5k). Most of the dust load is located in low layers (up to 2 km), while at higher layers (3-5 km) dust is underestimated by the model of about 0.02 km^{-1} MB but shows good agreement on fractional bias (Fig. 5o,s). Dust is also slightly (0.01km^{-1}) underestimated in regions of transport, northern and southern from the sources. Moving further eastwards at 30 – 50 º E, the dust originates from the Arabian desert (10 – 35º N) and is transported further southern towards the eastern Africa and northern towards Turkey (Fig. 5h). Dust extinction takes high values over the expanded area of Saudi Arabia, up to 1.5 km height and 0.11 km^{-1} and reaches heights of 5 km with 0.07 km^{-1} dust extinction values. The model significantly underestimates the dust extinction over the Arabian sources at the order of 0.08 km^{-1} especially at low altitudes up to 1 km, both in mean and fractional bias (Fig. 5 p-t). It is also not able to simulate well the dust transported over Iraq, Syria and Turkey over 32 – 40 ºN.

3.3. Evaluation of mean regional dust properties

Figure 6 displays the mean vertical distributions of the observed and simulated dust extinction for nine sub-regions of our study domain representing distinct dust characteristics: Eastern Tropical North Atlantic (15-22º W, 0-30º N), Eastern Subtropical North Atlantic (10-22º W, 30-60º N), Northern Europe (-10-40º E, 45-60º N), Western Mediterranean (-10-15º E, 30-45º N), Eastern Mediterranean (15-35º E, 30-45º N), Western Sahara (-15-10º E, 10-30º N), Eastern Sahara (10-35º E, 10-30º N), Northern Chad (10-22º E, 13-22º N) and Middle East (35-

50º E, 20-40º N). Based on our results, it is evident a variability of mineral particles' load vertical extension among the considered sub-domains. Maximum values of extinction (0.10km^{-1}) are observed over the dust source regions of Western Africa at altitudes lower than 500m, which gradually decrease for increasing heights up to 6km. Similar patterns are observed over the Eastern Sahara with maximum extinctions up to 0.07km^{-1}, while over Northern Chad the corresponding levels can be as high as 0.12km^{-1}. In the Middle East, the extinction levels are high near the ground (0.12km^{-1}) with standard deviation values up to 0.40km^{-1}. Dust is transported over the Mediterranean with maximum values of dust extinction of 0.03km^{-1} at the boundary layer while mineral particles are found up to 6km. Dust is further transported and detected over Northern Europe with low but still present values of extinction (maximum of 0.01 km^{-1} at the boundary layer). Low amounts of dust are also detected over the Eastern Subtropical North Atlantic and westerly over the Eastern Tropical North Atlantic with maximum values of extinction up to 0.06km^{-1}. The model captures the general patterns of dust emission and transportation over the area, although biases are also present. Over Western Africa the model simulates the maximum of extinction at about 200 m higher than observed, while in altitudes higher than 2 km dust extinction is underestimated. In Eastern Sahara, there is an overestimation at layers lower than 3 km and an underestimation at heights greater than 3 km. At the highly dust-active area of Northern Chad, the model simulates greater extinction coefficient compared to CALIPSO (maximum values of 0.17 to 0.12km^{-1} respectively). The maximum extinction at this area is observed at 500 m but simulated higher, at approximately 1km. Above 3 km height the model simulates lower extinction values than observed. Over Middle East there is an underestimation of dust along the vertical column, which is stronger for maximum values of extinction below 2 km height. Over Eastern Mediterranean the model underestimates dust near the surface, but simulates successfully the extinction from 1 km and up to 6 km height. Over Western Mediterranean the simulated dust profile is close to the observed with a slight underestimation of extinction at low layers (<500 m) and slight overestimation from 0.5 km up to 5 km of altitude. The model has difficulties in simulating the dust transported and reaching Northern Europe and Eastern Subtropical North Atlantic. The west transport over the Eastern Tropical North Atlantic is also underestimated by the model in all the atmospheric column simulating an almost constant extinction coefficient of 0.02km^{-1} from 0.3 up to 4 km height.

Figure 7 presents the statistical indicator's profile for each region as well as the corresponding number of profiles. The mean biases (Fig. 7a) show that the model simulates higher values of dust extinction over the Sahara dust sources compared to CALIPSO, this difference reaching maximum values of 0.04 km^{-1} (0.1 km^{-1} at Northern Chad) at about 1-2 km height, while at higher altitudes (4-6 km) the model underestimates the dust extinction. The transported dust over the Eastern Tropical North Atlantic is slightly overestimated (~0.007km^{-1}) by the model in low altitudes (<2 km) and underestimated (~0.01 km^{-1}) at 4-6km height. Over the Mediterranean, the dust extinction profile is overestimated (up to 0.01 km^{-1} for the Western Mediterranean and up to 0.003 km^{-1} for the Eastern Mediterranean). East Subtropical North Atlantic and Northern Europe present similar patterns with a slight overestimation of dust (<0.005 km^{-1}) at low altitudes (<3 km). The area of Middle East presents the highest underestimation of dust extinction coefficient starting from 0.04km^{-1} in low altitudes and decreasing with height. This is also shown in the RMSE profiles (Fig. 7b) where the greatest deviations between observations and model are present at the area of Middle East and Northern Chad and for low altitudes. In all regions the deviation is greater at low altitudes and

514 decreases with height. High differences (MB ≈ 0.15km^{-1}) are also present for the Sahara region.
515 On the contrary, low biases are present at the region of East Subtropical North Atlantic and
516 Northern Europe where the dust extinction is low. Most of the regions present a similar
517 correlation coefficient pattern (Fig. 7c) with maximum correlation (~0.6) at 4-5 km of altitude
518 corresponding both to areas with large number of profiles (Eastern Mediterranean, Sahara and
519 Middle East) and less profiles as well (East Tropical North Atlantic). The only region that
520 presents the same profile pattern but with smaller correlation values is North Europe with
521 maximum correlation of about 0.4. Above 5 km and below 3 km height the correlation decreases
522 and takes values lower than 0.5.

523 Further we compare the column-integrated dust properties for the regions of study. Figure 8
524 shows the Taylor's diagrams of the DOD and the center of mass for each region, where the
525 azimuthal angle presents the correlation coefficient, the distance from the point on the x-axis
526 presents the RMSE and the radial distance presents the standard deviation of the simulated
527 patterns. The dust optical depth (Fig. 8a) is better represented over the East Tropical North
528 Atlantic (r ~0.75 and RMSE~ 0.09). It is quite well represented over the strong dust sources of
529 Sahara and the Middle East, while the area of Northern Chad presents low correlation (r=0.5),
530 high RMSE (~0.19) and high standard deviation (~0.19). The worst simulation occurs for the
531 areas of rare dust events transported towards Northern Europe (r<0.3 and RMSE~0.2). The
532 region of Northern Europe and East Subtropical North Atlantic presents also the less good
533 simulations of the dust center of mass height (Fig. 8b) with r~0.4. The dust center of mass
534 height presents the better simulations over the Sahara (r~0.85, RMSE~0.6), the Middle East
535 (r~0.82, RMSE~0.7), and at the dust transport regions of East Tropical North Atlantic and the
536 Mediterranean Sea with better simulations over the western than the eastern Mediterranean.

537 The ability of the model to correctly simulate the temporal variation of dust is examined over
538 characteristic regions of the Eastern Sahara, Middle East and Western Mediterranean as typical
539 areas of dust generation and dust transport. Figure 9 shows the observed (red line) and
540 simulated (black line) interannual (upper diagrams) and intrannual (medium diagrams) variability
541 as well as the mean bias of the intrannual (lower diagrams) variability of the DOD (left column)
542 and the dust center of mass height (right column). The model captures the temporal variability of
543 dust at both source and transport areas, and at both interannual and intrannual scales. Over the
544 dust source regions of Eastern Sahara, the model simulates the picks during warm months,
545 although both overestimations and underestimations of less than 0.1 DOD take place (Fig. 9a).
546 Similarly, the model simulates the annual cycle of DOD with maximum values (~0.2) during April
547 to June and lower values between November and January. Low differences (<0.05) and within
548 the limits of the standard deviation are found between the model and the observations
549 (Fig.9b,c). The simulated dust center of mass height over Eastern Sahara follows the observed
550 temporal variability but is slightly (<200m) lower than the observed consistently throughout the
551 study period (Fig. 9d-f). Over the Middle East the model simulates the interannual and
552 intrannual variation of dust optical depth (Fig. 9g-i), but it constantly underestimates them,
553 missing especially the high values when dust activity peaks during spring and summer periods
554 (MB~0.13), while during summer 2009 this underestimation becomes greater (~0.2). Taking
555 also into consideration the fact that over the Middle East CALIPSO already mis-detects the high
556 values of optical depth compared to MODIS (Fig. A, values of AOD close to 1), we conclude that
557 the model has serious problem in simulating dust over the Middle East. Despite these limitations
558 the simulation of the dust center of mass height above Middle East presents significant
559 accordance with the observations (Fig. 9j-l). Regarding the transported dust over Western

Mediterranean the model simulates the temporal variability of the lower values of dust load (DOD<0.15) overestimating it slightly during warm months from March to June, except for the summer of 2012 (Fig. 9m-o). The variability of the dust center of mass height over the same region is also well simulated by the model (Fig. 9p-r) with a constant negative bias of about 200m.

4. Conclusions

In the present study, we evaluate the dust regional model BSC-DREAM8b based on the 3D LIVAS-CALIPSO dust product and assess the potential model biases. To this aim, we compare 5 years of observed and simulated dust extinction profiles (2009-2013) focusing on the northern Africa, the Mediterranean Sea, Europe, the Middle East and the Atlantic Ocean from 0 to 60º N and from 22º W to 50º E.

The aim of the study is to use the LIVAS-CALIPSO dust product as reference for the evaluation study and thus highlight that the product is key towards understanding the three-dimensional properties of dust and provides for the first time the ability to compare the simulated and observed dust structures over the entire model domain.

The BSC-DREAM8b performance in reproducing CALIPSO-derived mean dust extinction profiles showed that :

- The model follows similar to the observational patterns: the thickest layers are found during summer and over the emission areas and the dust masses shift from southern latitudes during autumn and winter to northern latitudes in spring and summer.
- The transported dust adjacent to the sources is underestimated by the model except for the dust transport over the Mediterranean Sea that is overestimated (maximum MB of extinction of 0.15km^{-1} over Western Mediterranean at 1-2km altitude).
- The dust center of mass height is slightly underestimated by the model over the Mediterranean by about 200m.
- We found an underestimation in extinction of dust transported at Northern Europe (MB of extinction ~ -0.005km^{-1}), and a low correlation with the observed DOD (r<0.4), due also to the small dust sampling over the region of Northern Europe.
- The model simulates less dust transported towards the Eastern Tropical North Atlantic all over the year (MB of DOD~-0.1), although the DOD has good correlation with the observed values and low RMSE (r~0.75, RMSE~0.9).
- There is a significant underestimation of dust over the Middle East all along the vertical column, being stronger during warm seasons and reaching up to -0.2 MB of DOD and up to -0.07km^{-1} MB of extinction. This underestimation being even stronger when considering that CALIPSO mid-detects DOD over this region. In addition, the RMSE of the dust extinction is high (up to 0.3km^{-1}) while

the temporal variation of the dust center of mass is very well simulated by the model over the area of Middle East.

A previous study of Basart et el. [2012] that evaluated BSC-DREAM8b with data from AERONET stations and from seasonally averaged passive satellite observations, has identified different model's biases compared to the results of the present study: that the model strongly underestimates AOD over the Sahel, overestimates the AOD over northwestern Africa, the Middle East and the Mediterranean in spring.

The results presented in this study help to constrain the model uncertainty which is very important to give information to the users about the accuracy of the provided dust forecasts. Such observational evidence on the vertical structure of dust plumes is provided for the first time and the evaluation methodology followed in this study highlights the importance of this information for the evaluation of regional dust models. An interesting finding is also produced from the quantitative comparisons between model and satellite extinctions showing a significant overestimation close to the strong Saharan sources (e.g. in Algeria and Bodelé). Such discrepancy between model and satellite data at these areas may also imply certain constraints of the CALIOP to detect the strong dust activity either due to misclassification of dust as clouds or due to the attenuation of the lidar signal in extreme events. Future developments in the observational dataset will focus on the mitigation of such issues.

Acknowledgements

The authors acknowledge support through

- the D-TECT project with ID 725698 of the ERC Consolidator Grant,

- the InDust COST Action CA16202

- the ECARS under grant agreement No 602014 from the European Union's Horizon 2020 Research and Innovation program.

- the AXA Research Fund for funding aerosol research at the Barcelona Supercomputing Center through the AXA Chair on Sand and Dust Storms.

- BSC-DREAM8b simulations were performed on the Mare Nostrum supercomputer hosted by the Barcelona Supercomputing Center (BSC).

- CALIPSO data were provided by NASA and were obtained from the ICARE Data Cente (http://www.icare.univ-lille1.fr/). We thank the ICARE Data and Services Center for providing access to the data used in this study and their computational centre. LIVAS product was produced under the ESA–ESTEC project LIVAS (contract no. 4000104106/11/NL/FF/fk) and improved under the European Union Seventh Framework Programme (FP7/2007–2013) project MarcoPolo (grant agreement no. 606953).

- Emmanouil Proestakis acknowledges the Stavros Niarchos Foundation for its support.

- Antonis Gkikas acknowledges the DUST-GLASS project funded from the European Union's Horizon 2020 research and Innovation programme under the Marie Skłodowska-Curie grant agreement No 749461.

References

Amiridis, V., Wandinger, U., Marinou, E., Giannakaki, E., Tsekeri, A., Basart, S., Kazadzis, S., Gkikas, A., Taylor, M., Baldasano, J., and Ansmann, A.: Optimizing CALIPSO Saharan dust retrievals, Atmos. Chem. Phys., 13, 12089-12106, doi:10.5194/acp-13-12089-2013, 2013.

Amiridis, V., Marinou, E., Tsekeri, A., Wandinger, U., Schwarz, A., Giannakaki, E., Mamouri, R., Kokkalis, P., Binietoglou, I., Solomos, S., Herekakis, T., Kazadzis, S., Gerasopoulos, E., Proestakis, E., Kottas, M., Balis, D., Papayannis, A., Kontoes, C., Kourtidis, K., Papagiannopoulos, N., Mona, L., Pappalardo, G., Le Rille, O., and Ansmann, A.: LIVAS: a 3-D multi-wavelength aerosol/cloud database based on CALIPSO and EARLINET, Atmos. Chem. Phys., 15, 7127-7153, https://doi.org/10.5194/acp-15-7127-2015, 2015.

Balkanski, Y., Schulz, M., Claquin, T., and Guibert, S.: Reevaluation of Mineral aerosol radiative forcings suggests a better agreement with satellite and AERONET data, Atmos. Chem. Phys., 7, 81–95, doi:10.5194/acp-7-81-2007, 2007.

Basart, S., Pérez, C., Nickovic, S., Cuevas, E., and Baldasano, J.: Development and evaluation of the BSCDREAM8b dust regional model over northern Africa, the Mediterranean and the Middle East, Tellus B, 64, 18539, doi:10.3402/tellusb.v64i0.18539, 2012.

Binietoglou, I., Basart, S., Alados-Arboledas, L., Amiridis, V., Argyrouli, A., Baars, H., Baldasano, J. M., Balis, D., Belegante, L., Bravo-Aranda, J. A., Burlizzi, P., Carrasco, V., Chaikovsky, A., Comerón, A., D'Amico, G., Filioglou, M., Granados-Muñoz,M. J., Guerrero-Rascado, J. L., Ilic, L., Kokkalis, P., Maurizi, A., Mona, L., Monti, F., Muñoz-Porcar, C., Nicolae, D., Papayannis, A., Pappalardo, G., Pejanovic, G., Pereira, S. N., Perrone, M. R., Pietruczuk, A., Posyniak, M., Rocadenbosch, F., Rodríguez-Gómez, A., Sicard, M., Siomos, N., Szkop, A., Terradellas, E., Tsekeri, A., Vukovic, A., Wandinger, U., and Wagner, J.: A methodology for investigating dust model performance using synergistic EARLINET/AERONET dust concentration retrievals, Atmos. Meas. Tech., 8, 3577–3600, doi:10.5194/amt-8-3577-2015, 2015.

Chen, S., Huang, J., Jiang, N., Zang, Z., Guan, X., Ma, X., Jia, Z., Zhang, X., Zhang, Y., Huang, K., Xu, X., Zhang, G., Li, J., Yang, R., and Liao, S.: Estimations of anthropogenic dust emissions at global scale from 2007 to 2010, Atmos. Chem. Phys. Discuss., https://doi.org/10.5194/acp-2017-890, under review, 2017.

Chen, S., J Huang,J. Li,R. Jia, N. Jiang, L. Kang, X. Ma, T. Xie, Comparison of dust emission, transport, and deposition between the Taklimakan Desert and Gobi Desert from 2007 to 2011, 2017, Science China Earth Sciences, 60:1-1, doi:1.01007/s11430-016-9051-0.

Colarco, P. R., Toon, O. B., Reid, J. S., Livingston, J. M., Russell, P. B., Redemann, J., Schmid, B., Maring, H. B., Savoie, D., Welton, E. J., Campbell, J. R., Holben, B. N. and Levy, R.: Saharan dust transport to the Caribbean during PRIDE: 2. Transport, vertical profiles, and deposition in simulations of in situ and remote sensing observations, J. Geophys. Res.-Atmos., 108(D19), 8590, doi:10.1029/2002JD002659, 2003

DeMott, P. J., Sassen, K., Poellot, M. R., Baumgardner, D., Rogers, D. C., Brooks, S. D., Prenni, A. J., and Kreidenweis, S. M.: African dust aerosols as atmospheric ice nuclei, Geophys. Res. Lett., 30, 1732, doi:10.1029/2003GL017410, 2003.

Engelstaedter, S., and R. Washington (2007), Atmospheric controls on the annual cycle of North African dust, J.Geophys. Res., 112, D03103, doi:10.1029/2006JD007195.

Gama, C., Tchepel, O., Baldasano, J. M., Basart, S., Ferreira, J., Pio, C., Cardoso, J. and Borrego, C.: Seasonal patterns of Saharan dust over Cape Verde-a combined approach using observations and modelling, Tellus B, 67, 24410, doi:10.3402/tellusb.v67.24410, 2015.

Ginoux, P., J. M. Prospero, O. Torres, and M. Chin (2004), Long-term simulation of global dust distribution with the GOCART model: Correlation with North Atlantic Oscillation, Environ. Modell. Software, 19, 113 – 128.

Ginoux, P., D. Garbuzov, and N. C. Hsu, 2010: Identification of anthropogenic and natural dust sources using Moderate Resolution Imaging Spectroradiometer (MODIS) Deep Blue level 2 data. J. Geophys. Res. Atmos., 115, D05204.

692 Ginoux, P., J. M. Prospero, T. E. Gill, N. C. Hsu, and M. Zhao (2012), Global-scale attribution of anthropogenic and
693 natural dust sources and their emission rates based on MODIS Deep Blue aerosol products, Rev. Geophys., 50,
694 RG3005, doi:10.1029/2012RG000388.
695 Gkikas, A., Basart, S., Hatzianastassiou, N., Marinou, E., Amiridis, V., Kazadzis, S., Pey, J., Querol, X., Jorba, O.,
696 Gassó, S., and Baldasano, J. M.: Mediterranean intense desert dust outbreaks and their vertical structure based
697 on remote sensing data, Atmos. Chem. Phys., 16, 8609-8642, https://doi.org/10.5194/acp-16-8609-2016, 2016.
698 Haustein, K., Pérez, C., Baldasano, J. M., Müller, D., Tesche, M. and co-authors. 2009. Regional dust model
699 performance during SAMUM 2006. *Geophys. Res. Lett*. **36**, L03812.
700 Huang, J., Q. Fu, J. Su, et al., 2009: Taklimakan dust aerosol radiative heating derived from CALIPSO observations
701 using the Fu-Liou radiation model with CERES constraints. Atmos. Chem. Phys., 9, 4011-4021, doi: 10.5194/acp-
702 9-4011-2009.
703 Janjic, Z. I. 1977. Pressure gradient force and advection scheme used for forecasting with steep and small scale
704 topography. *Contr. Atmos. Phys.* **50**, 186–199.
705 Janjic, Z. I. 1979. Forward-backward scheme modified to prevent twogrid-interval noise and its application in sigma
706 coordinate models. *Contr. Atmos. Phys.* 52, 69–84.
707 Janjic, Z. I. 1984. Non-linear advection schemes and energy cascade on semi-staggered grids. *Mon. Weather Rev.*
708 **112**, 1234–1245.
709 Janjic, Z. I. 1990. The step-mountain coordinate: physical package. *Mon. Weather Rev.* **118**, 1429–1443.
710 Janjic, Z. I. 1994. The step-mountain eta coordinate model: further developments of the convection, viscous sublayer,
711 and turbulence closure schemes. *Mon. Weather Rev.* **122**, 927–945.
712 Janjic, Z. I. 1996a. *The Mellor-Yamada Level 2.5 Turbulence Closure Scheme in the NCEP Eta Model, in Research*
713 *Activities in Atmospheric and Oceanic Modelling, CAS/WGNE*, 4.14–4.15. World Meteorological Organization,
714 Geneva.
715 Janjic, Z. I. 1996b. The surface layer parameterization in the NCEP Eta Model. In: *Research Activities in Atmospheric*
716 *and Oceanic Modelling, CAS/C WGNE*, 4.16–4.17. World Meteorological Organization, Geneva.
717 Jiménez-Guerrero, P., Pérez, C., Jorba, O. and Baldasano, J. M. 2008. Contribution of Saharan dust in an integrated
718 air quality system and its on-line assessment. Geophys. Res. Lett. 35, L03814.
719 Kipling, Z., P. Stier, J. P. Schwarz, A. E. Perring, J. R. Spackman, G. W. Mann, C. E. Johnson, and P. J. Telford
720 (2013), Constraints on aerosol processes in climate models from vertically-resolved aircraft observations of black
721 carbon, Atmos. Chem. Phys., 13, 5969-5986, doi:10.5194/acp-13-5969-2013.
722 Kipling, Z., P. Stier, C. E. Johnson, G. W. Mann, N. Bellouin, S. E. Bauer, T. Bergman, M. Chin, T. Diehl, S. J. Ghan,
723 T. Iversen, A. Kirkevåg, H. Kokkola, X. Liu, G. Luo, G. Myhre, T. v. Noije, K. J. Pringle, K. v. Salzen, M. Schulz, Ø.
724 Seland, T. Takemura, K. Tsigaridis and K. Zhang (2015), What controls the vertical distribution of aerosol?
725 Relationships between process sensitivity in HadGEM3–UKCA and inter-model variation from AeroCom Phase II,
726 Atmos. Chem. Phys. Discuss., 15, 25933-25980.
727 Kittaka, C., Winker, D. M., Vaughan, M. A., Omar, A., and Remer, L. A.: Intercomparison of column aerosol optical
728 depths from CALIPSO and MODIS-Aqua, Atmos. Meas. Tech., 4, 131–141, doi:10.5194/amt-4-131-2011, 2011.
729 Klein, H., Nickovic, S., Haunold, W., Bundke, U., Nillius, B., Ebert, M., Weinbruch, S., Schuetz, L., Levin, Z., Barrie, L.
730 A., and Bingemer, H.: Saharan dust and ice nuclei over Central Europe, Atmos. Chem. Phys., 10, 10211–10221,
731 doi:10.5194/acp10-10211-2010, 2010.
732 Knippertz, P., and M. C. Todd (2010), The central west Saharan dust hot spot and its relation to African easterly
733 waves and extratropical disturbances, J. Geophys. Res., 115, D12117, doi:10.1029/2009JD012819.
734 Kosmopoulos, P. G., Kazadzis, S., Taylor, M., Athanasopoulou, E., Speyer, O., Raptis, P. I., Marinou, E., Proestakis,
735 E., Solomos, S., Gerasopoulos, E., Amiridis, V., Bais, A. and Kontoes, C.: Dust impact on surface solar irradiance
736 assessed with model simulations, satellite observations and ground-based measurements, Atmos. Meas. Tech.,
737 10(7), doi:10.5194/amt-10-2435-2017, 2017.
738 Li, W.; El-Askary, H.; ManiKandan, K.P.; Qurban, M.A.; Garay, M.J.; Kalashnikova, O.V. Synergistic Use
739 of Remote Sensing and Modeling to Assess an Anomalously High Chlorophyll-*a* Event during Summer
740 2015 in the South Central Red Sea. *Remote Sens.* 2017, *9*, 778.
741 Liu, Z., Omar, A., Vaughan, M., Hair, J., Kittaka, C., Hu, Y., Powell, K., Trepte, C., Winker, D., Hostetler, C., Ferrare,
742 R., and Pierce, R.: CALIPSO lidar observations of the optical properties of Saharan dust: A case study of long-
743 range transport, J. Geophys. Res., 113, D07207, doi:10.1029/2007JD008878, 2008.
744 Ma, X., Bartlett, K., and Yu, F.: Comparison of AOD between CALIPSO and MODIS: significant differences over
745 major dust and biomass burning regions, Atmos. Meas. Tech., 6, 2391-2401, 2013, doi: 10.5194/amt-6-2391-
746 2013
747 Mahowald, N. M., et al., 2010: Observed 20th century desert dust variability: Impact on climate and biogeochemistry.
748 Atmos. Chem. Phys., 10, 10875–10893
749 Marinou, E., Amiridis, V., Binietoglou, I., Tsikerdekis, A., Solomos, S., Proestakis, E., Konsta, D., Papagiannopoulos,
750 N., Tsekeri, A., Vlastou, G., Zanis, P., Balis, D., Wandinger, U., and Ansmann, A.: Three-dimensional evolution of

Saharan dust transport towards Europe based on a 9-year EARLINET-optimized CALIPSO dataset, Atmos. Chem. Phys., 17, 5893-5919, doi:10.5194/acp-17-5893-2017, 2017.
Markaki Z. , Oikonomou K. , Kocak M. , Kouvarakis G. , Chaniotaki A. , Kubilay N. , Mihalopoulos N. , (2003), Atmospheric deposition of inorganic phosphorus in the Levantine Basin, eastern Mediterranean: Spatial and temporal variability and its role in seawater productivity, Limnology and Oceanography, 4, doi: 10.4319/lo.2003.48.4.1557.
Mesinger, F., Janjic, Z. I., Nickovic, S., Gavrilov, D. and Deaven, D. G. 1988. The step-mountain coordinate: model description and performance for cases of Alpine lee cyclogenesis and for a case of an Appalachian redevelopment. *Mon. Weather Rev.* 116, 1493–1518.
Mikami, M., et al. (2006), Aeolian dust experiment on climate impact: An overview of Japan China joint project ADEC, Global Planet. Change, 52, 142 – 172, doi:10.1016/j.gloplacha.2006.03.001.
Mona, L., Papagiannopoulos, N., Basart, S., Baldasano, J., Binietoglou, I., Cornacchia, C., and Pappalardo, G.: EARLINET dust observations vs. BSC-DREAM8b modeled profiles: 12-year-long systematic comparison at Potenza, Italy, Atmos. Chem.Phys., 14, 8781–8793, doi:10.5194/acp-14-8781-2014, 2014.
Mulitza, S., et al., 2010: Increase in African dust flux at the onset of commercial agriculture in the Sahel region. Nature, 466, 226–228.
Myhre, G., D. Shindell, F.-M. Bréon, W. Collins, J. Fuglestvedt, J. Huang, D. Koch, J.-F. Lamarque, D. Lee, B. Mendoza, T. Nakajima, A. Robock, G. Stephens, T. Takemura and H. Zhang, 2013: Anthropogenic and Natural Radiative Forcing. In: Climate Change 2013: The Physical Science Basis. Contribution of Working Group I to the Fifth Assessment Report of theIntergovernmental Panel on Climate Change [Stocker, T.F., D. Qin, G.-K. Plattner, M. Tignor, S.K. Allen, J. Boschung, A. Nauels, Y. Xia, V. Bex and P.M. Midgley (eds.)]. Cambridge University Press, Cambridge, United Kingdom and New York, NY, USA
Nickovic, S., Kallos, G., Papadopoulos, A. and Kakaliagou, O. 2001. A model for prediction of desert dust cycle in the atmosphere. J. Geophys. Res. 106, 18113–18130.
Nisantzi, A., Mamouri, R. E., Ansmann, A., Schuster, G. L., and Hadjimitsis, D. G.: Middle East versus Saharan dust extinction-to-backscatter ratios, Atmos. Chem. Phys., 15, 7071-7084, https://doi.org/10.5194/acp-15-7071-2015, 2015.
Omar, A., Winker, D., Kittaka, C., Vaughan, M., Liu, Z., Hu, Y. X., Trepte, C., Rogers, R., Ferrare, R., Lee, K., Kuehn, R., and Hostetler, C.: The CALIPSO automated aerosol classification and lidar ratio selection algorithm, J. Atmos. Ocean. Tech., 26, 1994–2014, doi:10.1175/2009jtecha1231.1, 2009.
Omar, A. H., Winker, D. M., Tackett, J. L., Giles, D. M., Kar, J., Liu, Z., Vaughan, M. A., Powell, K. A., and Trepte, C. R.: CALIOP and AERONET aerosol optical depth comparisons: One size fits none, J. Geophys. Res.-Atmos., 118, 4748–4766, doi:10.1002/jgrd.50330, 2013.
Pappalardo, G., et al. (2010), EARLINET correlative measurements for CALIPSO: First intercomparison results, J. Geophys. Res., 115, D00H19, doi:10.1029/2009JD012147.
Papayannis, A., et al. (2008), Systematic lidar observations of Saharan dust over Europe in the frame of EARLINET (2000–2002), J. Geophys. Res., 113, D10204, doi:10.1029/2007JD009028.
Park, S.-U., and J.I. Jeong, 2018: Direct radiative forcing due to aerosols in Asia during March 2002. Sci. Total Environ., 407, 394-404, doi: 10.1016/j.scitotenv.2008.07.041.
Pay, M. T., Piot, M., Jorba, O., Gassó, S., Gonçalves, M. and co-authors. 2010. A full year evaluation of the CALIOPE-EU air quality modeling system over Europe for 2004. *Atmos. Environ*. **44**, 3322–3342.
Pérez, C., Nickovic, S., Pejanovic, G., Baldasano, J. M. and Ozsoy, E. 2006. Interactive dust-radiation modeling: a step to improve weather forecasts. *J. Geophys. Res.* **11**, D16206.
Proestakis, E., Amiridis, V., Marinou, E., Georgoulias, A. K., Solomos, S., Kazadzis, S., Chimot, J., Che, H., Alexandri, G., Binietoglou, I., Daskalopoulou, V., Kourtidis, K. A., de Leeuw, G., and van der A, R. J.: 9-year spatial and temporal evolution of desert dust aerosols over South and East Asia as revealed by CALIOP, Atmos. Chem. Phys. Discuss., https://doi.org/10.5194/acp-2017-797, in review, 2017., Submitted for publication in ACP, MS No.: acp-2017-797.
Prospero, J. M., K. Barrett, T. Church, F. Dentener, R. A. Duce, J. N. Galloway, H. Levy, J. Moody, and P. Quinn (1996), Atmospheric deposition of nutrients to the North Atlantic Basin, Biogeochemistry, 35, 27– 73.
Prospero, J. M., P. Ginoux, O. Torres, S. E. Nicholson, and T. E. Gill (2002), Environmental characterization of global sources of atmospheric soil dust identified with the NIMBUS 7 total ozone mapping spectrometer (TOMS) absorbing aerosol products, Rev. Geophys., 40(1), 1002, doi:10.1029/2000RG000095.
Rodríguez, S., Cuevas, E., Prospero, J. M., Alastuey, A., Querol, X., López-Solano, J., García, M. I., and Alonso-Pérez, S.: Modulation of Saharan dust export by the North African dipole, Atmos. Chem. Phys., 15, 7471-7486, https://doi.org/10.5194/acp-15-7471-2015, 2015.
Samset, B.H., G. Myhre, M. Schulz, Y. Balkanski, S. E. Bauer, T. K. Berntsen, H. Bian, N. Bellouin, T. Diehl, R. C. Easter, S. J. Ghan, T. Iversen, S. Kinne, A. Kirkevåg, J.-F. Lamarque, G. Lin, X. Liu, J. Penner, Ø. Seland, R. B.

Skeie, P. Stier, T. Takemura, K. Tsigaridis, and K. Zhang (2013), Black carbon vertical profiles strongly affect its radiative forcing uncertainty, Atmos. Chem. Phys., 13, 2423-2434, doi:10.5194/acp-13-2423-2013.

Schuster, G. L., Vaughan, M., MacDonnell, D., Su, W., Winker, D., Dubovik, O., Lapyonok, T., and Trepte, C.: Comparison of CALIPSO aerosol optical depth retrievals to AERONET measurements, and a climatology for the lidar ratio of dust, Atmos. Chem. Phys., 12, 7431–7452, doi:10.5194/acp-12-7431-2012, 2012.

Sokolik, I. N. and Toon, O. B.: Direct radiative forcing by anthropogenic airborne mineral aerosols, Nature, 381, 681–683, 1996.

Solomos, S., Ansmann, A., Mamouri, R.-E., Binietoglou, I., Patlakas, P., Marinou, E., and Amiridis, V.: Remote sensing and modelling analysis of the extreme dust storm hitting the Middle East and eastern Mediterranean in September 2015, Atmos. Chem. Phys., 17, 4063-4079, https://doi.org/10.5194/acp-17-4063-2017, 2017.

Solomos, S., Kallos, G., Kushta, J., Astitha, M., Tremback, C., Nenes, A., and Levin, Z.: An integrated modeling study on the effects of mineral dust and sea salt particles on clouds and precipitation, Atmos. Chem. Phys., 11, 873–892, doi:10.5194/acp11-873-2011, 2011.

Tackett, J. L., Winker, D. M., Getzewich, B. J., Vaughan, M. A., Young, S. A., and Kar, J.: CALIPSO lidar level 3 aerosol profile product: version 3 algorithm design, Atmos. Meas. Tech. Discuss., https://doi.org/10.5194/amt-2018-97, in review, 2018.

Tegen, I., and A. A. Lacis (1996), Modeling of particle size distribution and its influence on the radiative properties of mineral dust aerosol, J. Geophys. Res., 101(D14), 19237–19244, doi:10.1029/95JD03610.

Tesche, M., Ansmann, A., Müller, D., Althausen, D., Engelmann, R., Freudenthaler, V., and Grob, S.: Vertically Resolved Separation of Dust and Smoke over Cape Verde Using Multiwavelength Raman and Polarization Lidars during Saharan Mineral Dust Experiment 2008, J. Geophys. Res., 114, D13202, doi:10.1029/2009JD011862, 2009.

Textor, C., M. Schulz, S. Guibert, S. Kinne, Y. Balkanski, S. E. Bauer, T. Berntsen, T. Berglen, O. Boucher, M. Chin, F. Dentener, T. Diehl, R. Easter, H. Feichter, D. Fillmore, S. Ghan, P. Ginoux, S. Gong, A. Grini, J. Hendricks, L. Horowitz, P. Huang, I. Isaksen, I. Iversen, S. Kloster, D. Koch, A. Kirkevåg, J. E. Kristjansson, M. Krol, A. Lauer, J.-F Lamarque, X. Liu, V. Montanaro, G. Myhre, J. Penner, G. Pitari, S. Reddy, Ø. Seland, P. Stier, T. Takemura, and X. Tie (2006), Analysis and quantification of the diversities of aerosol life cycles within AeroCom, Atmos. Chem. Phys., 6, 1777–1813, doi:10.5194/acp-6-1777-2006.

Todd, M. C. 2008. Quantifying uncertainty in estimates of mineral dust flux: an intercomparison of model performance over the Bodélé Depression, Northern Chad. *J. Geophys. Res.* **113**, D24107.

Tsikerdekis, A., Zanis, P., Steiner, A. L., Solmon, F., Amiridis, V., Marinou, E., Katragkou, E., Karacostas, T., and Foret, G.: Impact of dust size parameterizations on aerosol burden and radiative forcing in RegCM4, Atmos. Chem. Phys., 17, 769-791, https://doi.org/10.5194/acp-17-769-2017, 2017.

Wang, Y., Sartelet, K. N., Bocquet, M., Chazette, P., Sicard, M.,D'Amico, G., Léon, J. F., Alados-Arboledas, L., Amodeo, A.,Augustin, P., Bach, J., Belegante, L., Binietoglou, I., Bush, X.,Comerón, A., Delbarre, H., García-Vízcaino, D., Guerrero-Rascado, J. L., Hervo, M., Iarlori, M., Kokkalis, P., Lange, D., Molero, F., Montoux, N., Muñoz, A., Muñoz, C., Nicolae, D.,Papayannis, A., Pappalardo, G., Preissler, J., Rizi, V., Rocaden-bosch, F., Sellegri, K., Wagner, F., and Dulac, F.: Assimilationof lidar signals: application to aerosol forecasting in the western Mediterranean basin, Atmos. Chem. Phys., 14, 12031–12053,doi:10.5194/acp-14-12031-2014, 2014.

Winker, D. M., Vaughan, M. A., Omar, A. H., Hu, Y., Powell, K. A., Liu, Z., Hunt, W. H., and Young, S. A.: Overview of the CALIPSO Mission and CALIOP Data Processing Algorithms, J. Atmos. Oceanic Technol., vol 26, pp. 2310–2323, doi: 10.1175/2009JTECHA1281.1, 2009.

Winker, D. M., J. Pelon, J. A. Coakley, Jr., S. A. Ackerman, R. J.Charlson, P. R. Colarco, P. Flamant, Q. Fu, R. Hoff, C. Kittaka, T. L.Kubar, H. LeTreut, M. P. McCormick, G. Megie, L. Poole, K. Powell, C.Trepte, M. A. Vaughan, B. A. Wielicki (2010), The CALIPSO mission: A global 3D view of aerosols and clouds. Bull. Amer. Meteor. Soc., 91, 1211–1229.

Yu, H., Chin, M., Winker, D. M., Omer, A. H., Liu, Z., Kittaka, C., and Diehl, T.: Global view of aerosol vertical distribution from CALIPSO lidar measurements and GOCART simulations: Regional and seasonal variations, J. Geophys. Res., 115, D00H30, doi:10.1029/2009JD013364, 2010.

Zhang, L., Gong, S., Padro, J. and Barrie, L. 2001. A size-segregated particle dry deposition scheme for an atmospheric aerosol module. *Atmos. Environ.* **35**, 549–560.

Zhao, Q. and Carr, F. H. 1997. A prognostic cloud scheme for operational NWP models. *Mon. Weather Rev.* **125**, 1931–1953.

Zhang, Z., Chen, B., Huang, J., Liu, J., Bi, J., Zhou, T., and Huang, Z.: Comparison of the optical properties of pure and transported anthropogenic dusts measured by ground-based Lidar, Atmos. Chem. Phys. Discuss., https://doi.org/10.5194/acp-2017-1000, under review, 2017.

Zhu, A., V. Ramanathan, F. Li, and D. Kim (2007), Dust plumes over the Pacific, Indian, and Atlantic oceans: Climatology and radiative impact, J. Geophys. Res., 112, D16208, doi:10.1029/2007JD008427.

List of Figures

extinction coefficient (in km^{-1}) for the different regions defined in Fig. 6, for the period 2009-2013. d) Histogram of the number of profiles corresponding to each region.

Figure 8: Taylor diagrams for BSC-DREAM8b model against the CALIPSO dust product for the regions defined in Fig.6 for the mean dust AOD and b) for the center of mass (in km) for the period 2009-2013. The radial distance from the origin is proportional to the standard deviation of a pattern. The centered root mean square error (RMSE) distance between the modeled and the observational field is proportional to their distance apart (in the same units as the standard deviation). The correlation between the two fields is given by the azimuthal position of the modeled field.

Figure 9: Temporal series of the interannual (upper lines), intrannual (medium lines) and mean bias of the intrannual (lower lines) variability of the BSC-DREAM8b modelled (black line) versus the observed by the CALIPSO (red line) AOD dust product (left column) and center of mass height (in km, right column), over Eastern Sahara (a-f), Middle East (g-l) and Western Mediterranean (m-r) for 2009-2013. In the mean bias the red areas correspond to overestimation and the blue areas to underestimation by the model.

Figure A: Spatial distribution of a) the mean dust optical depth observed by the CALIPSO dust product and b) the total aerosol optical depth observed by MODIS daily colocated with CALIPSO overpasses, for the domain between 22°W to 50°E and 0 to 60° N and for the period 2009-2013. Grey dotes denote lack of CALIPSO measurements.

Figure B: Spatial distribution of the mean dust optical depth as observed by the CALIPSO (first line), modelled by BSC-DREAM8b (second line), the mean bias (third line), and the fractional bias (fourth line) between the model and the observations for the domain between 22°W to 50°E and 0 to 60° N and for the period 2009-2013 . The first column (a,e,i,m) presents only the model outputs that correspond to CALIPSO overpasses, the second column (b,f,j) presents all the model outputs, the third column (c,g,k,h) corresponds to day time observations and simulations for the CALIPSO overpasses and the fourth column (d,h,l,o) corresponds only to night time observations and simulations for the CALIPSO overpasses. Grey dotes denote lack of CALIPSO measurements.

Figures

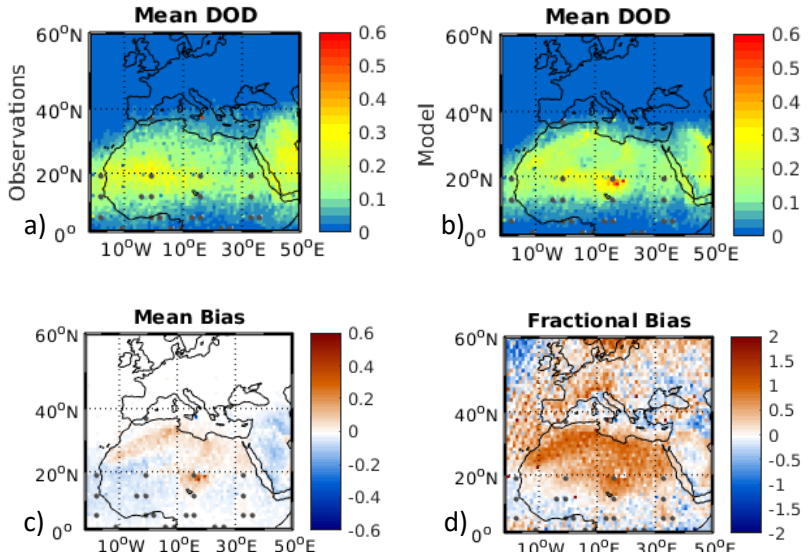

Figure 1: Spatial distribution of the mean dust optical depth a) observed by the CALIPSO dust product and b) modelled by BSC-DREAM8b, and (c) mean bias, (d) fractional bias, (e) correlation coefficient and (f) root mean square error for the domain between 22°W to 50°E and 0° to 60° N. The data are averaged for the 2009-2013 period. Grey dotes denote lack of CALIPSO measurements.

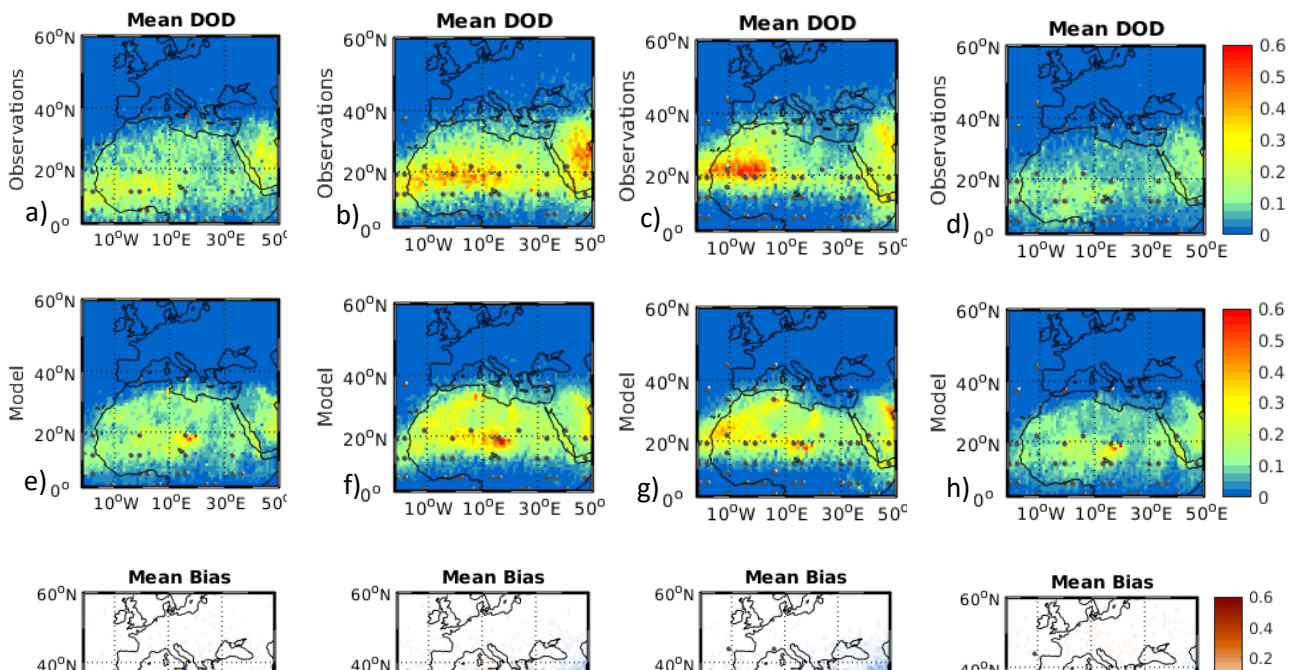

Figure 2: Seasonal spatial distribution of the mean dust optical depth as observed by the CALIPSO dust product (a-d), modeled by BSC-DREAM8b (e-h), the mean bias (i-l), and the fractional bias (m-p) between the model and the observations, for January - March (first column), April - June (second column), July - September (third column) and October – December (fourth column) for the domain between 22°W to 50°E and 0 to 60° N and for the period 2009-2013. Grey dotes denote lack of CALIPSO measurements.

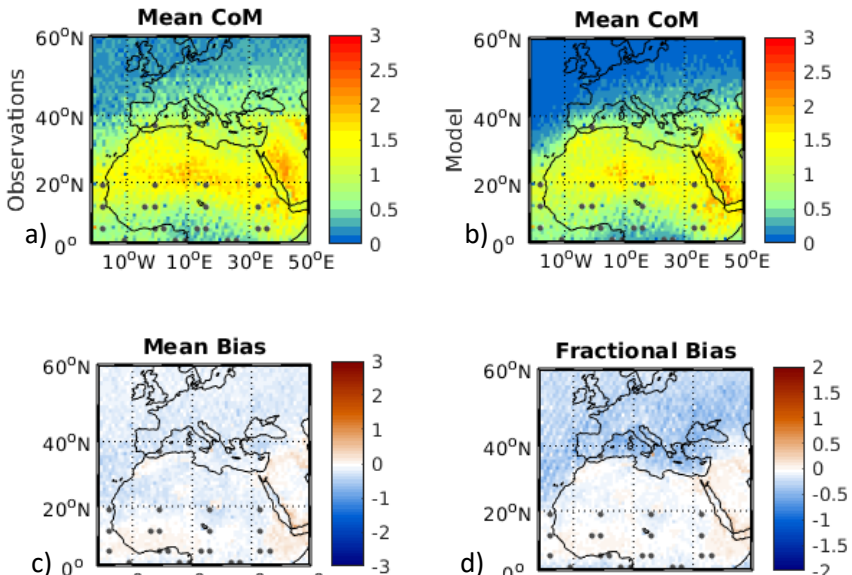

Figure 3: As in Fig. 1 for the center of mass (in km).

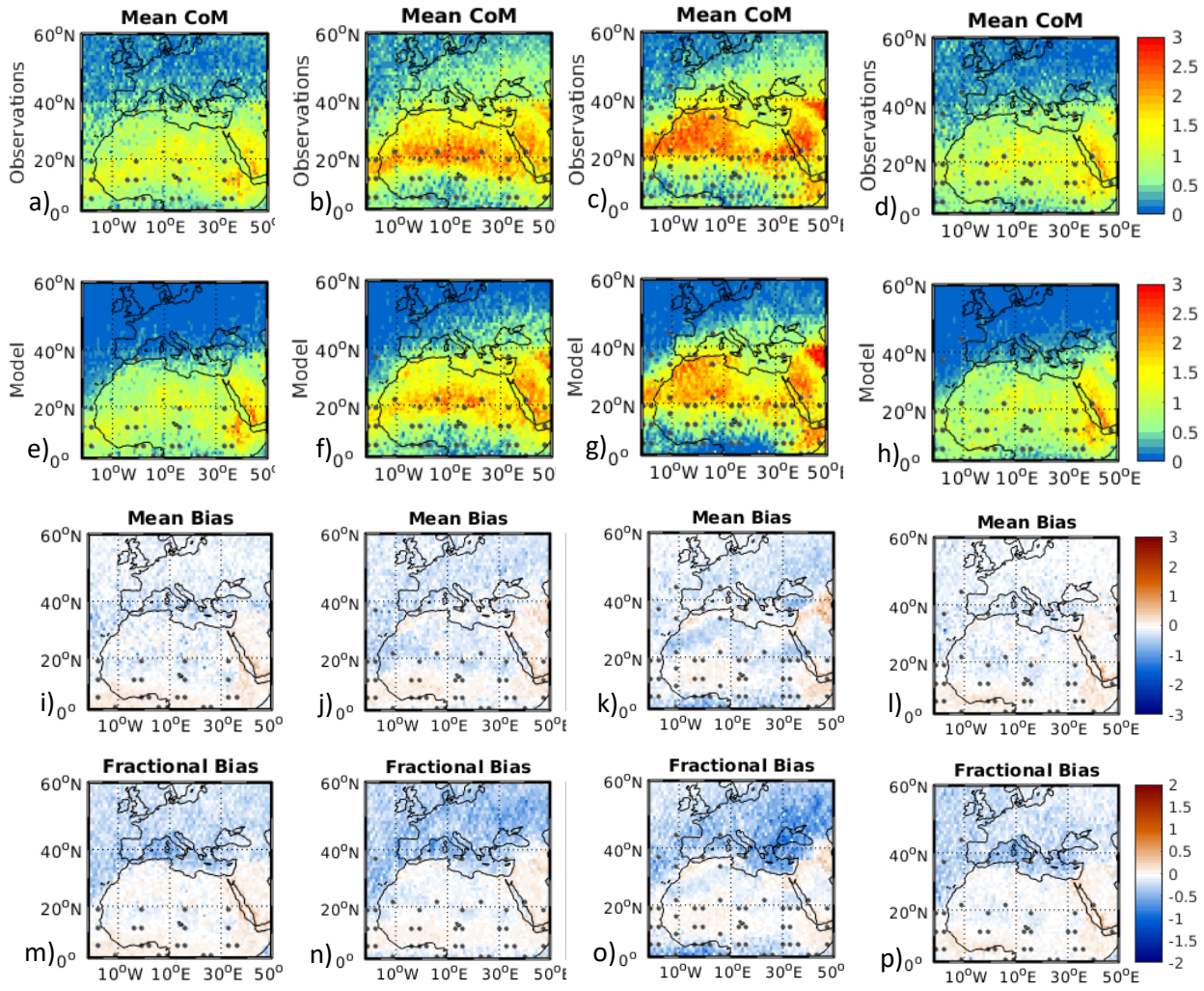

Figure 4: As in Fig. 2 for the center of mass (in km).

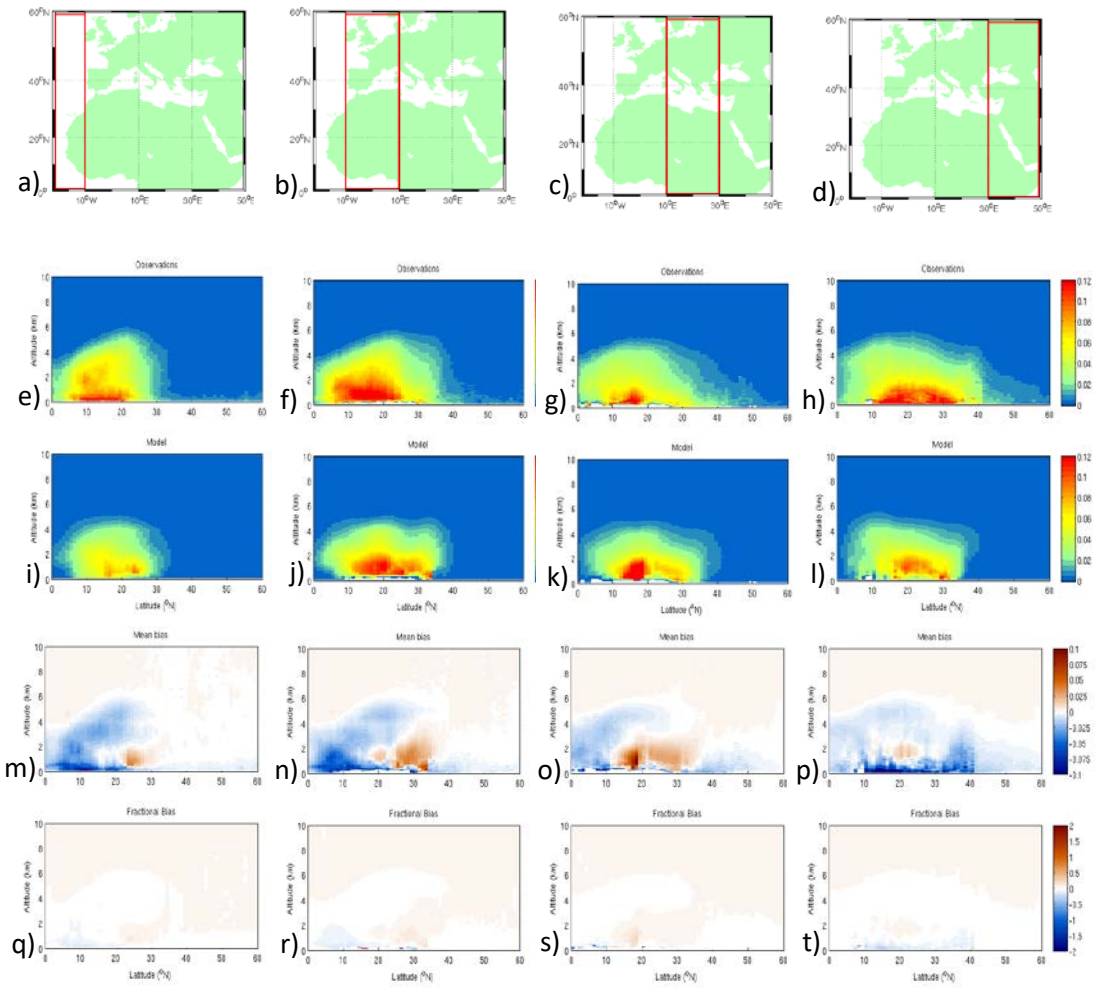

Figure 5: Zonal mean dust extinction coefficient (in km^{-1}) for the longitudinal regions from 22ºW to 50ºE as illustrated by domain maps (a-d), observed by the CALIPSO dust product (e-h), modeled by BSC-DREAM8b (i-l), the mean (m-p) and the fractional (q-t) bias between model and observations for the regions 22 to 10º W (a,e,i,m,q), 10º W to 10º E (b,f,j,n,r), 10 to 30º E (c,g,k,o,s) and 30 to 50º E (d,h,l,p,t) for the period 2009-2013.

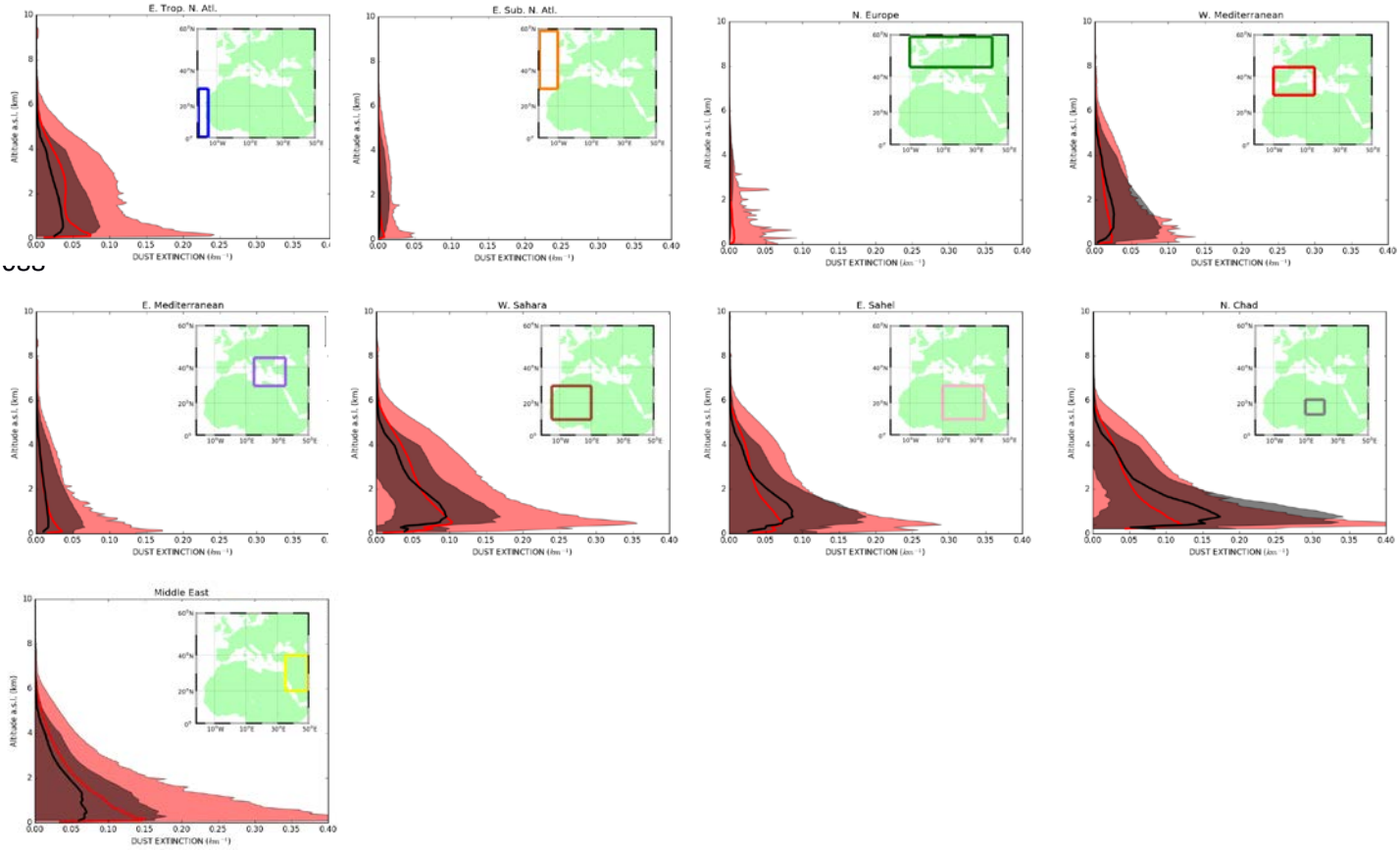

Figure 6: Mean profile of the dust extinction coefficient (in km^{-1}) as observed by the CALIPSO dust product (red line) and modeled by BSC-DREAM8b (black line) averaged by regions shown in the upper right map of each figure: Eastern Tropical North Atlantic (15-22º W, 0-30º N), Eastern Subtropical North Atlantic (10-22º W, 30-60º N), Northern Europe (-10-40º E, 45-60º N), Western Mediterranean (-10-15º E, 30-45º N), Eastern Mediterranean (15-35º E, 30-45º N), Western Sahara (-15-10º E, 10-30º N), Eastern Sahara (10-35º E, 10-30º N), Northern Chad (10-22º E, 13-22º N) and Middle East (35-50º E, 20-40º N), for the period 2009-2013. Shaded areas indicate the standard deviation of the mean values.

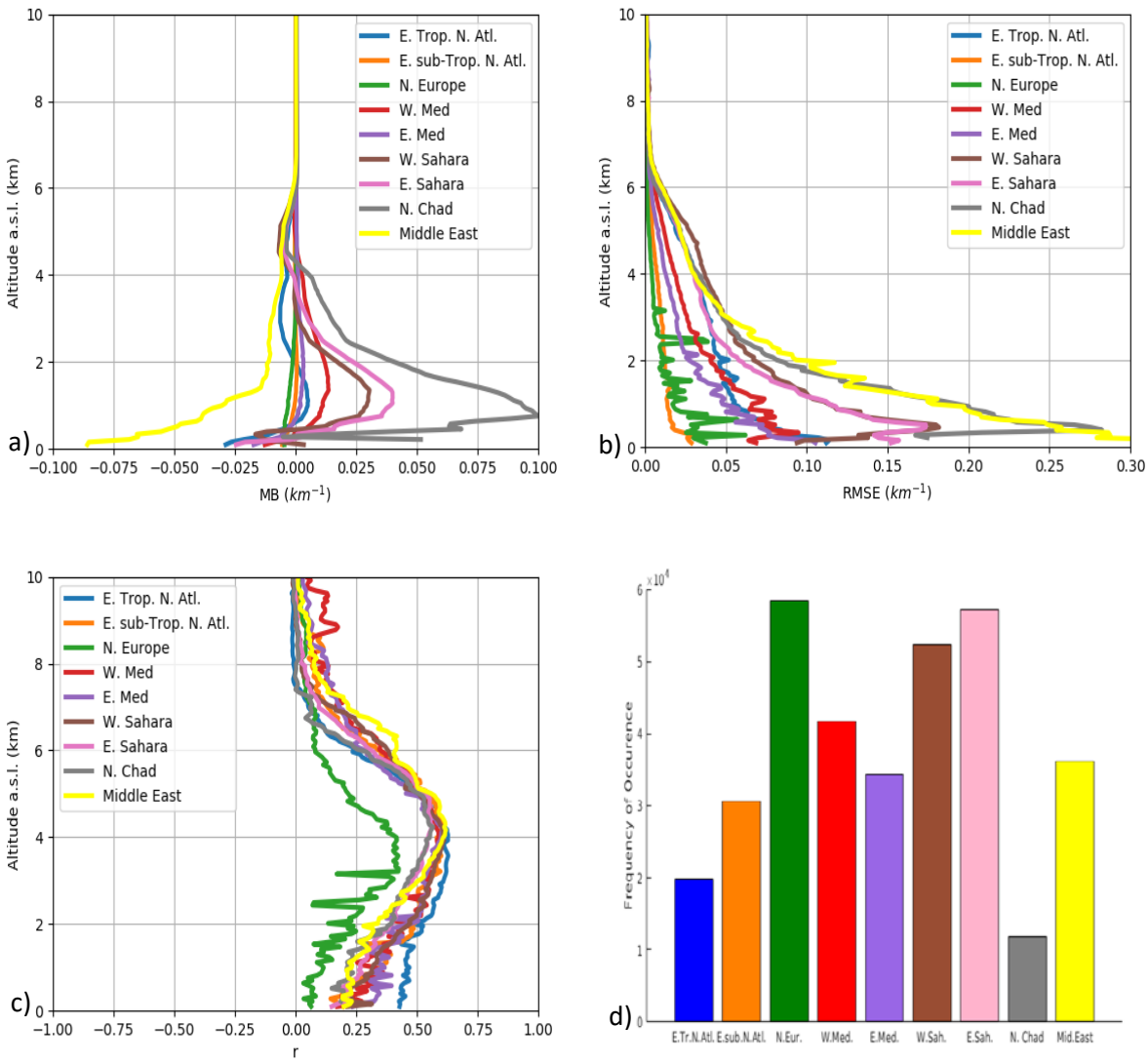

Figure 7: a) Mean bias, b) Root mean square error and c) Correlation coefficient between the observed by the CALIPSO dust product and the modeled by BSC-DREAM8b profiles of the dust extinction coefficient (in km^{-1}) for the different regions defined in Fig. 6, for the period 2009-2013. d) Histogram of the number of profiles corresponding to each region.

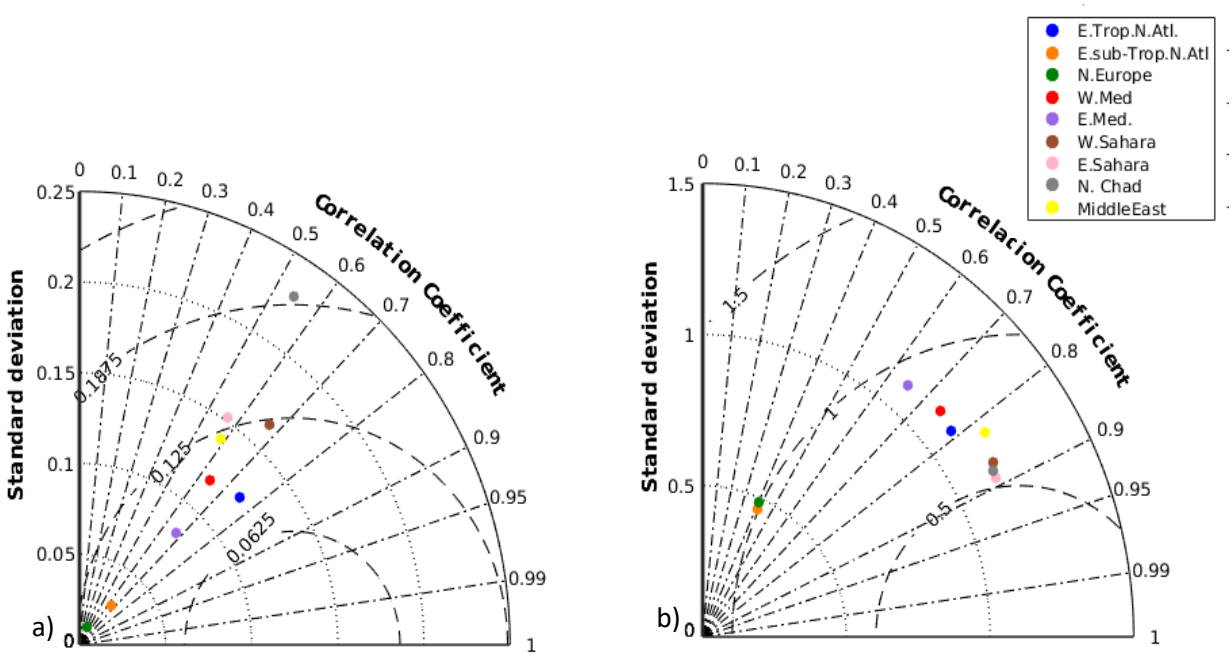

Figure 8: Taylor diagrams for BSC-DREAM8b model against the CALIPSO dust product for the regions defined in Fig.6 for the mean dust AOD and b) for the center of mass (in km) for the period 2009-2013. The radial distance from the origin is proportional to the standard deviation of a pattern. The centered root mean square error (RMSE) distance between the modeled and the observational field is proportional to their distance apart (in the same units as the standard deviation). The correlation between the two fields is given by the azimuthal position of the modeled field.

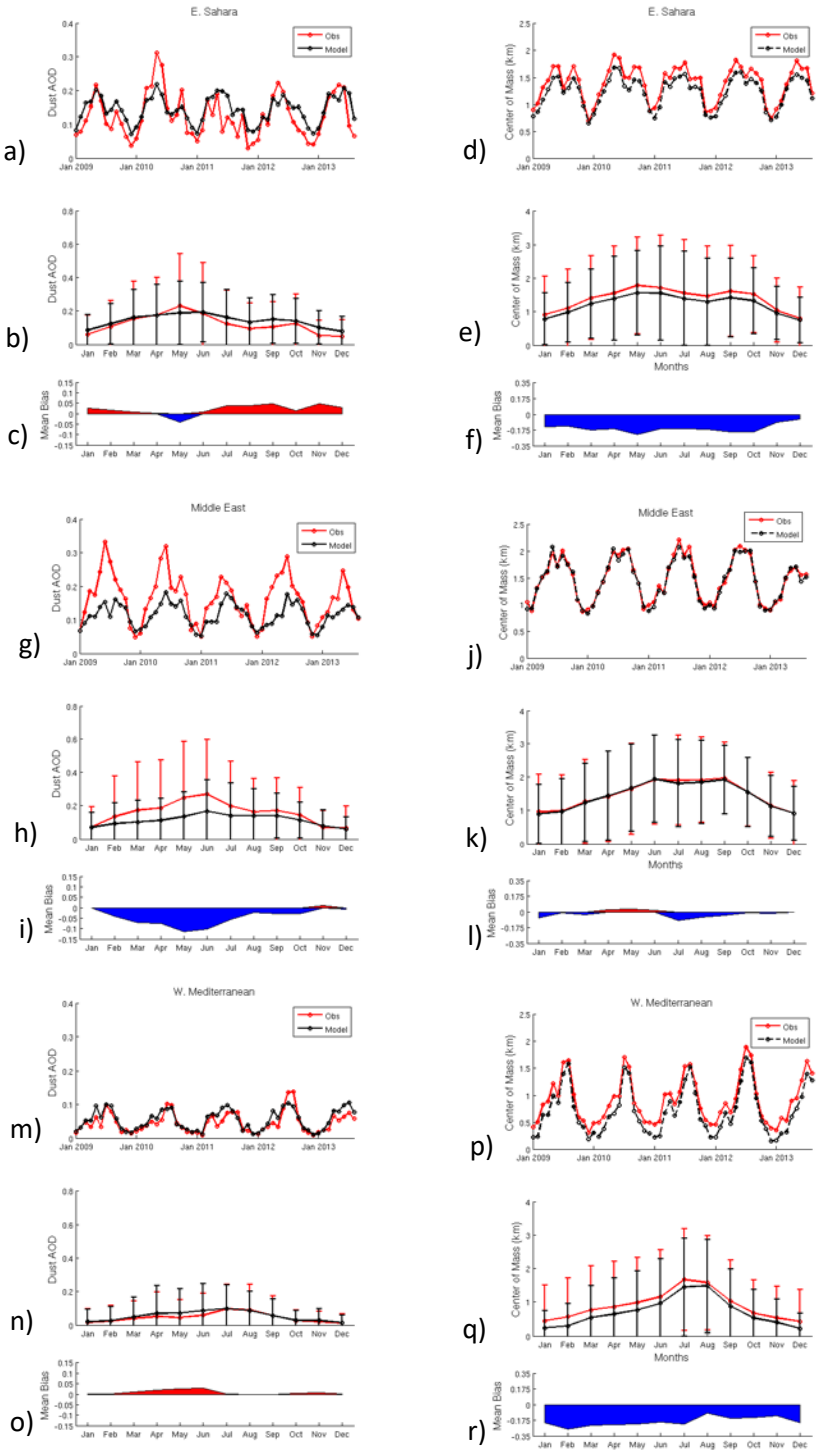

Figure 9: Temporal series of the interannual (upper lines), intrannual (medium lines) and mean bias of the intrannual (lower lines) variability of the BSC-DREAM8b modelled (black line) versus the observed by the CALIPSO (red line) AOD dust product (left column) and center of mass height (in km, right column), over Eastern Sahara (a-f), Middle East (g-l) and Western Mediterranean (m-r) for 2009-2013. In the mean bias the red areas correspond to overestimation and the blue areas to underestimation by the model.

Appendix

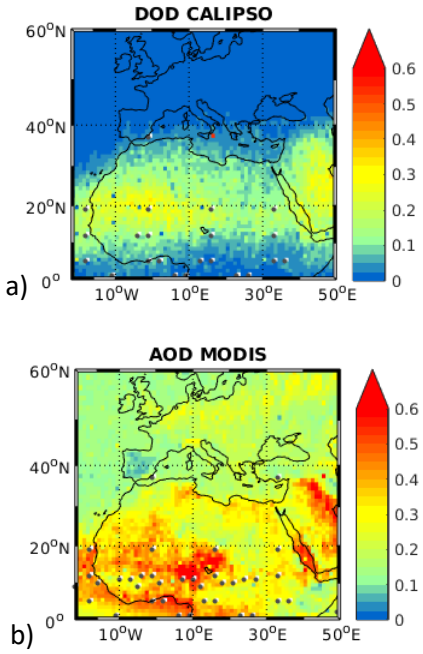

Figure A: Spatial distribution of a) the mean dust optical depth observed by the CALIPSO dust product and b) the total aerosol optical depth observed by MODIS daily colocated with CALIPSO overpasses, for the domain between 22°W to 50°E and 0 to 60° N, for the period 2009-2013. Grey dotes denote lack of CALIPSO measurements.

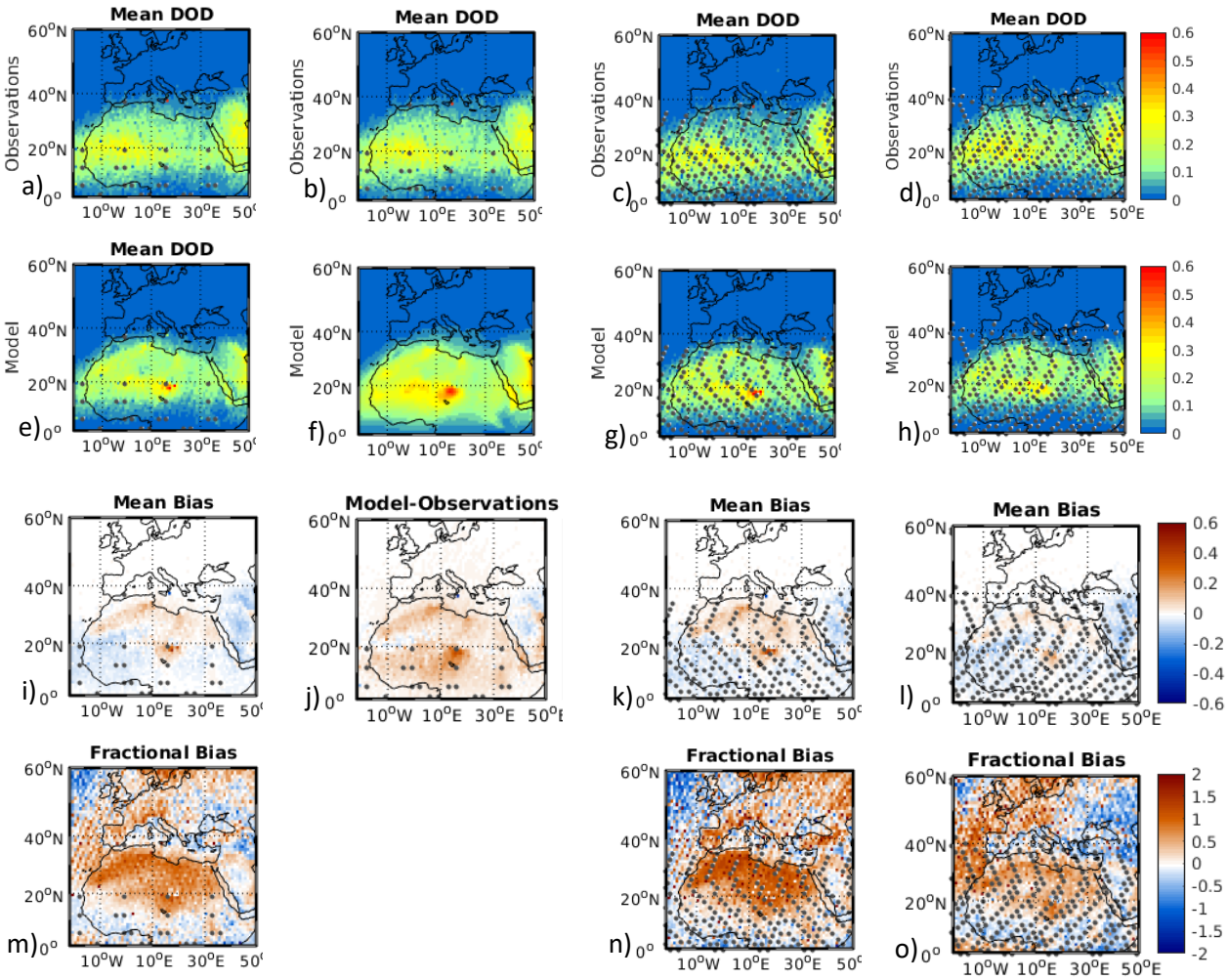

Figure B: Spatial distribution of the mean dust optical depth as observed by the CALIPSO (first line), modelled by BSC-DREAM8b (second line), the mean bias (third line), and the fractional bias (fourth line) between the model and the observations for the domain between 22°W to 50°E and 0 to 60° N and for the period 2009-2013. The first column (a,e,i,m) presents only the model outputs that correspond to CALIPSO overpasses, the second column (b,f,j) presents all the model outputs, the third column (c,g,k,h) corresponds to day time observations and simulations for the CALIPSO overpasses and the fourth column (d,h,l,o) corresponds only to night time observations and simulations for the CALIPSO overpasses. Grey dotes denote lack of CALIPSO measurements.